Endocrinology, 2022, **163**, 1–16
https://doi.org/10.1210/endocr/bqac127
Advance access publication 7 August 2022
Research Article

Androgen-mediated Perturbation of the Hepatic Circadian System Through Epigenetic Modulation Promotes NAFLD in PCOS Mice

Sambit Roy,[1,*] Aierken Abudu,[1,*] Irving Salinas,[1,*] Niharika Sinha,[1] Holly Cline-Fedewa,[1] Alexandra M. Yaw,[1] Wenjie Qi,[2] Todd A. Lydic,[3] Diana L. Takahashi,[4] Jon D. Hennebold,[5,6] Hanne M. Hoffmann,[1] Jianrong Wang,[7] and Aritro Sen[1]

[1]Reproductive and Developmental Sciences Program, Department of Animal Science, Michigan State University, East Lansing, MI, USA
[2]Department of Biomedical Engineering, Michigan State University, East Lansing, MI, USA
[3]Collaborative Mass Spectrometry Core, Department of Physiology, Michigan State University, East Lansing, MI, USA
[4]Division of Cardiometabolic Health
[5]Division of Reproductive & Developmental Sciences, Oregon National Primate Research Center, Beaverton, OR, USA
[6]Department of Obstetrics & Gynecology, Oregon Health & Science University, Portland, OR, USA
[7]Department of Computational Mathematics, Science and Engineering, Michigan State University, East Lansing, MI, USA

*These authors contributed equally.
Correspondence: Aritro Sen, PhD, Reproductive and Developmental Sciences Program, Department of Animal Sciences, 766 Service Rd, Interdisciplinary Science & Technology Building, Michigan State University, East Lansing, MI 48824, USA. Email: aritros@hotmail.com.

Abstract

In women, excess androgen causes polycystic ovary syndrome (PCOS), a common fertility disorder with comorbid metabolic dysfunctions including diabetes, obesity, and nonalcoholic fatty liver disease. Using a PCOS mouse model, this study shows that chronic high androgen levels cause hepatic steatosis while hepatocyte-specific androgen receptor (AR)-knockout rescues this phenotype. Moreover, through RNA-sequencing and metabolomic studies, we have identified key metabolic genes and pathways affected by hyperandrogenism. Our studies reveal that a large number of metabolic genes are directly regulated by androgens through AR binding to androgen response element sequences on the promoter region of these genes. Interestingly, a number of circadian genes are also differentially regulated by androgens. In vivo and in vitro studies using a circadian reporter [Period2::Luciferase (Per2::LUC)] mouse model demonstrate that androgens can directly disrupt the hepatic timing system, which is a key regulator of liver metabolism. Consequently, studies show that androgens decrease H3K27me3, a gene silencing mark on the promoter of core clock genes, by inhibiting the expression of histone methyltransferase, Ezh2, while inducing the expression of the histone demethylase, JMJD3, which is responsible for adding and removing the H3K27me3 mark, respectively. Finally, we report that under hyperandrogenic conditions, some of the same circadian/metabolic genes that are upregulated in the mouse liver are also elevated in nonhuman primate livers. In summary, these studies not only provide an overall understanding of how hyperandrogenism associated with PCOS affects liver gene expression and metabolism but also offer insight into the underlying mechanisms leading to hepatic steatosis in PCOS.

Key Words: PCOS, androgen, androgen receptor, liver, circadian clock, NAFLD

Polycystic ovary syndrome (PCOS) affects 10% to 15% of women worldwide (1-3) and primarily causes anovulation and fertility problems. However, PCOS women also develop or are more likely to develop diseases such as nonalcoholic fatty liver disease (NAFLD), type 2 diabetes, hypertension, and cardiovascular problems (4). Currently, the origin or underlying mechanism of PCOS is unknown, and the PCOS patient population is also highly heterogeneous, including lean and obese PCOS patients. However, hyperandrogenism represents the main attribute of PCOS (5, 6). Evidence from human (7-11) and animal (12, 13) studies establish that androgens in excess play a key role in PCOS etiology that significantly contributes to the development of the large number of comorbidities such as reproductive, endocrine, metabolic, and psychological dysfunctions (14, 15) associated with PCOS (16, 17).

NAFLD is one of the most common chronic noncommunicable diseases in the Western world. Defined as the accumulation of fatty acid content greater than 5% of liver weight, NAFLD is a spectrum of diseases ranging from steatosis (fat accumulation) involving increased de novo synthesis of lipids and fatty acids to nonalcoholic steatohepatitis, which is characterized by hepatic injury and inflammation and, with time, may progress to cirrhosis. Several studies have shown a link between PCOS and development of liver dysfunction such as NAFLD (18-20). Yet, direct androgen effects on liver metabolism and its manifestation as liver dysfunction in PCOS women are poorly understood. NAFLD in PCOS patients has been primarily viewed as a secondary outcome of obesity and/or insulin resistance that are often associated with hyperandrogenism. However, lean (21) and normal-weight (19) women with PCOS also have an increased rate of

Received: 5 May 2022. **Editorial Decision:** 3 August 2022. **Corrected and Typeset:** 27 August 2022

NAFLD (22, 23). Epidemiological studies show that in addition to body mass index and dysglycemia, androgen excess is also a contributing risk factor for NAFLD development in PCOS (24, 25). A recent meta-analysis study reported that the association of PCOS with a high risk of NAFLD is independent of obesity but correlates with hyperandrogenism (20). Similarly, other studies in PCOS patients have reported that hyperandrogenism, independent of insulin resistance, is significantly associated with the development of NAFLD in PCOS patients (26-28). While it is well established that obesity and/or insulin resistance causes NAFLD (29) and are a significant contributing factors in the development of liver dysfunction in PCOS, the concept that androgens can also directly affect liver function leading to NAFLD is now being considered.

Using a well-established dihydrotestosterone (DHT)-induced PCOS mouse model, this study determines the direct impact of elevated androgen levels on liver steatosis. We report that hepatocyte-specific androgen receptor knockout (hepARKO) rescues the hepatic steatosis phenotype in the PCOS mouse model. Furthermore, RNA-sequencing (RNA-seq) and metabolomic analyses show key metabolic genes and pathways downstream of androgen actions in the PCOS liver. Our results show that high androgen levels associated with PCOS through epigenetic modifications disrupt the hepatic circadian system resulting in changes in the expression of metabolic genes associated with liver dysfunction and steatosis. Furthermore, we report similar hepatic gene expression pattern between PCOS mouse model and nonhuman primates (rhesus macaques) receiving PCOS level of testosterone. Androgen actions are mediated by nuclear and/or extranuclear signaling (30-32), and previous studies (33-35) in the ovary from our laboratory have shown that the physiological effects of androgens are mediated through a synergistic effect between these AR signaling pathways. Similar to our previous studies in the liver, we show that the androgen-induced modulation of the hepatic circadian system involves both the nuclear and extranuclear AR signaling. In summary, this study offers a comprehensive understanding and molecular insight into the effect of hyperandrogenism on liver metabolism and the development of NAFLD associated with PCOS.

Material and Methods

Ethics Statement

Mouse studies were performed in accordance with the guidelines for the care and use of laboratory animals and were approved by the Institutional Animal Care and Use Committee at Michigan State University (approval no. PROTO202000156). The rhesus macaque studies were conducted according to the National Institutes of Health Guide for the Care and Use of Laboratory Animals. All protocols were approved by Oregon National Private Research Center's (ONPRC's) Institutional Animal Care and Use Committee.

Development of PCOS Mouse Model

Postnatal day 20-21 mice of comparable body weight were randomly divided into 2 groups (DHT and control) and were implanted subcutaneously with a 90-day continuous DHT release pellet (2.5 mg of DHT; Innovative Research of America) (36). Control mice were implanted with a placebo pellet. Mice were euthanized at the end of the treatment period (90 days). PCOS phenotype was determined by measuring estrous cyclicity through vaginal smears, taken daily for the last 30 days of treatment as described previously (36). Ovarian morphology was determined using hematoxylin- and eosin-stained paraffin-embedded ovarian sections and previously published criteria (36, 37).

Generation of hepARKO Mice

To generate hepARKO mice, AR (exon 2) floxed mice (38) were mated with albumin-Cre (Alb-Cre) mice (Jackson laboratory, strain: B6.Cg-Speer6-$^{ps1Tg(Alb\text{-}cre)21Mgn}$/J). The Alb-Cre transgene has been used extensively to drive hepatocyte-specific recombination of a gene of interest (39). First AR-loxP$^{flox/flox}$ females were crossed with Alb-Cre males. Thereafter, the Alb-Cre/+;AR-loxP$^{flox/Y}$ males were backcrossed with AR-loxP$^{flox/flox}$ females to generate Alb-Cre/+;AR-loxP$^{flox/flox}$ female mice conditionally deleted for AR in the hepatocytes. Genomic DNA was isolated from 18-day-old animals, and polymerase chain reaction (PCR) genotyping with appropriate primers was used to identify mice with wildtype (Wt), floxed, and cre transgene, revealing bands of 830, 930, and 390 bp, respectively. Once female mice reached 21 days of age, a 90-day continuous DHT release pellet (2.5 mg of DHT; Innovative Research of America) (36) or placebo pellets were inserted into the hepARKO mice under the skin.

Triglycerides Level in Liver

Livers were cut into small pieces, and 150 to 200 mg was used to measure triglyceride levels using a triglyceride colorimetric assay kit (Fisher, NC9656167) at 540 nm readout. Triglyceride concentrations were normalized to total protein concentration and are expressed as milligrams per deciliter.

Tissue Histology Oil Red Oil Staining Assay

Liver samples were fixed overnight in 4% paraformaldehyde for cryosections (40). Cryosections (8-µm thick) were stained with Oil Red O (Abcam, ab150678). Briefly, cryosections were warmed at room temperature for 3 minutes and were then put into 100% propylene glycol. Oil Red Oil staining was done for 10 minutes. The sections were differentiated in 85% propylene glycol and counterstained with Mayer's Hematoxylin Solution (Abcam, ab150678).

Metabolomics

Liver samples (~50 mg, 5 liver samples from 5 different animals/treatment, DHT vs placebo) were subjected to biphasic extraction using a modified Folch chloroform/methanol/water extraction, as previously described (41) with the recovery of polar and semipolar metabolites in the aqueous upper extraction phase. Twenty nanograms of stable isotope-labeled (D4)-glycochenodeoxycholic acid were added to each sample during extraction for use in the estimation of metabolite recovery and for relative quantitation across experimental groups. Extracts were dried in a SpeedVac centrifuge and reconstituted in 200 µL of acetonitrile.

The liquid chromatography-mass spectrometry (LC-MS) platform consisted of a Shimadzu Prominence high-performance liquid chromatography coupled to a Thermo Scientific LTQ-Orbitrap Velos mass spectrometer. The liquid chromatography system included 2 LC20AD pumps, a vacuum degassing system, an autosampler, and a column

oven. The high-performance liquid chromatography column was a Phenomenex 2.0 mmx100 mm HILIC (3 microns, 100 Angstrom pore size) column equipped with a guard cartridge of the same column chemistry. Solvent A was water containing 50 mM ammonium formate. Solvent B was acetonitrile. The flow rate was 200 µL per minute, and the column oven was held at 25°C with the autosampler at 4°C and 5 µL of each sample was injected. The gradient conditions used were time 0 to 2 minutes, 95% solvent B. Column eluant was diverted to waste using a 2-position 6-port valve for the first 1.5 minutes. From time 2 minutes to 14 minutes, Solvent B was decreased linearly to 50% and then held at 50% for 5 minutes. The column was then re-equilibrated at 95% solvent B for 10 minutes. Column eluent was introduced to a Thermo LTQ-Orbitrap Velos mass spectrometer via a heated electrospray ionization source. The mass spectrometer was operated in negative ion mode at 60 000 resolution using the Fourier transform analyzer for full-scan MS data, and data-dependent product ion spectra were collected on the 4 most abundant ions at 7500 resolution using the Fourier transform analyzer. The electrospray ionization source was maintained at a spray voltage of 4.5 kV with sheath gas at 30 (arbitrary units) and auxiliary gas at 10 (arbitrary units). The inlet of the mass spectrometer was held at 350°C, and the S-lens were set to 35%. The heated electrospray ionization source was maintained at 350°C. Chromatographic alignment, isotope correction, peak identification, and peak area calculations were performed using MAVEN and XCMS software. Peak areas were normalized against the D4-glychochenodeoxycholic acid internal standard. Analyte m/z and retention times were compared against reference standards using MAVEN software, and unknown LC-MS peaks generated by XCMS software were searched for potential matches against the KEGG online database. Statistical analysis was performed using MetaboAnalyst software (www.metaboanalyst.ca).

Western Blot Analysis

Western blots were performed as described previously (42-44). Antibodies used were mouse anti-EZH2 (45), rabbit anti-JMJD3 (46), rabbit anti-RPL19 (47), rabbit anti-H3K27me3 (48), rabbit anti-H3 (49), rabbit anti-AR (50), and rabbit anti-BMAL1 (51). All antibodies used were at 1:1000 dilution.

RNA Isolation and RNA-seq

Total RNA isolation, library construction, and RNA-seq services were carried out by Genewiz, Inc, as described previously (34, 44). For RNA-seq, total RNA was extracted from liver tissues isolated from placebo and DHT pelleted animals (n = 3 liver samples from 3 different mice/treatment) using Qiagen RNeasy Plus Universal mini kit following the manufacturer's instructions (Qiagen, Hilden, Germany). RNA samples were quantified using Qubit 2.0 Fluorometer (Life Technologies, Carlsbad, CA, USA) and RNA integrity was checked using Agilent TapeStation 4200 (Agilent Technologies, Palo Alto, CA, USA). RNA integrity number for all the samples was between 9.7 to 10. RNA-seq libraries were prepared using 500 ng RNA, and the NEBNext Ultra RNA Library Prep Kit for Illumina, following the manufacturer's instructions (NEB, Ipswich, MA, USA). The sequencing library was validated on the Agilent TapeStation (Agilent Technologies, Palo Alto, CA, USA) and quantified by using Qubit 2.0 Fluorometer (Invitrogen, Carlsbad, CA, USA), as well as by quantitative PCR (KAPA Biosystems, Wilmington, MA, USA). The sequencing libraries were clustered on a single lane of a flow cell. After clustering, the flow cell was loaded on the Illumina HiSeq instrument (4000 or equivalent) according to the manufacturer's instructions. The samples were sequenced using a 2 × 150 bp paired-end configuration. The total number of reads/sample was 45 to 50 million. Image analysis and base calling were conducted by the HiSeq Control Software. Raw sequence data (.bcl files) generated from Illumina HiSeq were converted into fastq files and demultiplexed using Illumina's bcl2fastq 2.17 software. One mismatch was allowed for index sequence identification.

Bioinformatics Analysis for RNA-seq

Raw data quality was judged based on Illumina's Q score, which represents the error rate at each base, built on a log10 score. Thereafter, sequence reads were trimmed to remove possible adapter sequences and nucleotides with poor quality using Trimmomatic v.0.36. The trimmed reads were mapped to the reference *Mus musculus* GRCm38 genome available on ENSEMBL using the STAR aligner v.2.5.2b. The STAR aligner uses a spliced aligner that detects splice junctions and incorporates them to help align the entire read sequences. BAM files were generated as a result of this step. Unique gene hit counts were calculated using feature Counts from the Subread package v.1.5.2. Only unique reads that fell within exon regions were counted. After extraction of gene hit counts, the gene hit counts table was used for downstream differential expression analysis. Using DESeq2 R package, differentially expressed genes (DEGs) were identified between placebo (n = 3) and DHT pelleted (n = 3). The heat maps were constructed using log-transformed values obtained from RNA-seq data followed by z-normalization. The Wald test was used to generate *P*-values, and the Benjamini-Hochberg test was used for adjusted *P*-value. Genes with adjusted *P*-values ≤ 0.05 and absolute log2 fold changes > 0.5 were called DEGs for each comparison. For gene ontology analysis, significant DEGs were clustered by their gene ontology, and the enrichment of gene ontology terms was tested using Fisher exact test (GeneSCF v1.1-p2). Pathways with *P*-values ≤ 0.05 were considered significant. A list of all the DEGs is shown in the supplemental (Table 1) (52). The RNA-seq data are available in the Gene Expression Omnibus (accession no. GSE197765) (https://www.ncbi.nlm.nih.gov/geo/query/acc.cgi?acc=GSE197765).

Quantitative Real-Time PCR

Quantitative real-time PCR (qRT-PCR) was performed by Δ/ΔCt method as described previously (34, 43) using 1 µg of RNA for all the qRT-PCR reactions with TaqMan gene expression assay primers (assay IDs: Mm00840032_m1-Kdm5c, Mm00432554_m1-Cidea, Mm00617672_m1-Cidec, Mm00840165_g1-Fgf21, Mm00500223_m1-Arntl, Mm00440940_m1-Ppar-γ, Mm01204084_m1-Ppp1r3c, Mm00442759_m1-Chka, Mm00475794_m1-Plin2, Mm00475772_m-Adcy6, Mm00455950_m1-clock, Mm00503358_m1-Mogat1, Mm00507980_m1-Agxt, Mm01351475_g1-Hint2). Each target gene was normalized to *Rpl19* (Mm02601633_g1-Rpl19). For Rhesus monkey, gene expressions primers used were Rh01555643_m1-Arntl, Rh02897526_g1-Clock, Rh00985430_m1-Hmgcs2, Rh04254609_g1-Ddit3, Rh02787680_m1-Ppar-γ, Rh07255046_m1-Fgf2, and Rh02852283_m1-Mogat1. Each target gene was normalized to *Rpl32* (Rh02811772_s1-Rpl32).

Chromatin Immunoprecipitation Assay

A chromatin immunoprecipitation assay (ChIP) was performed using the MAGnify Chromatin Immunoprecipitation System (Invitrogen) as previously described (34, 43, 44, 53). Chromatin fragments were immunoprecipitated with Dynabeads coupled with rabbit anti-H3K27me3 ChIP grade antibody (54), rabbit anti-AR ChIP grade antibody (50), and rabbit anti-BMAL1 ChIP grade antibody (51). Rabbit immunoglobin G as a nonspecific control and 1 µg per ChIP reaction were used. Quantitative PCR was performed using PerfeCTa SYBR Green Supermix, ROX (VWR, cat no. 95055-500) with primers designed within 1000 bp from transcription start sites (TSS; identified using the Eukaryotic Promoter Database) of the mouse promoters.

In Vitro and In Vivo Liver Tissue Recordings of Per2::LUC Expression

All LumiCycle studies were carried out in female Per2::LUC circadian reporter mice (Jackson Laboratory, strain: B6.129S6-*Per2*^{tm1Jt}/J) (55). For in vivo studies, Per2::LUC mice were inserted with a 90-day continuous DHT release pellet (2.5 mg of DHT; Innovative Research of America) (36), and livers were removed after 90 days of DHT pellet treatment. Control mice were implanted with a placebo pellet. For in vitro studies, 6-week-old Per2::LUC mice (untreated) were used. For both the in vitro and in vivo experiment, the liver was removed immediately and placed in ice-cold Hanks' Balanced Salt Solution for approximately 30 to 60 minutes. Small (~3 × 2 mm) liver sections were placed individually on a 30-mm MilliCell membrane (Millipore-Sigma) in a 35-mm cell culture dish containing Dulbecco's modified Eagle's medium with high glucose (no phenol red), 10 µM N-2-hydroxyethylpiperazine-N′-2-ethane sulfonic acid, 1% penicillin/streptomycin, 2% B27 supplement, and 1 mM luciferin (BD Biosciences). For the in vitro studies, liver sections were treated with media alone (control) or 25 nM or 1 µM DHT. The lid was sealed to the plate using vacuum grease to ensure an airtight seal. Plated tissues were loaded into a LumiCycle luminometer (Actimetrics) inside a 35°C nonhumidified incubator at ZT6-6.5, and recordings were started. The bioluminescence was counted for 70 seconds every 10 minutes for 6 days (day 1-7 of recording time). Per2::LUC rhythm data were analyzed using LumiCycle Analysis software (Actimetrics) by an experimenter blind to the experimental group. To allow the tissue to recover and stabilize from sectioning, the data collected from the first 24 hours of culture were not included in the data analysis. Data were normalized by subtraction of the first 24 hours and fitted to a dampened sine wave (LM fit, damped) model. The period was defined as the time in hours between the peaks of the fitted curve. Amplitude was defined as the amplitude of the fitted sine wave. Phase relationships were analyzed via Rayleigh test of uniformity and a Watson's 2-sample test of homogeneity or a 1-criterion analysis of variance for circular data, followed by pairwise comparisons, and Watson's 2-sample test of homogeneity using Bonferroni's correction to accommodate family-wise error rate, where appropriate. Phase data were reported in radians with circular mean deviation.

miR-101 Isolation and Detection

Total RNA was isolated using the standard Trizol isolation method according to the manufacturer's instructions, and RT-PCR was performed using the TaqMan MicroRNA Reverse Transcription Kit and mouse *miR-101* TaqMan MicroRNA Assays (assay ID-002507; ThermoFisher Scientific). *snoRNA202* (assay ID-001232; ThermoFisher Scientific) was used as endogenous control, and relative expression of *miR-101* was calculated using the Δ/ΔCt method.

Nonhuman Primate PCOS Model

Liver samples from nonhuman primate (female rhesus macaques) PCOS model were obtained from Oregon Primate Center, Oregon Health and Science University (Portland, OR, USA). Female rhesus macaques at 2.5 years of age were treated with cholesterol implants (controls) or testosterone implants (mean serum levels: 1.35 ± 0.01 ng/mL) as described previously (56, 57) for 5 years prior to collection of liver samples used in this study.

Statistical Analysis

Statistical analysis was performed using GraphPad Prism version 7 (GraphPad Software) and RStudio 2021.09.2 + 382 "Ghost Orchid" release. Statistical comparisons were made by paired/unpaired Student's *t*-test (for comparing 2 groups), a 1-way analysis of variance followed by Dunnett's (for comparing multiple groups). Results with $P < 0.05$ were considered significant.

Results

Direct Androgen Actions Through the Hepatic Androgen Receptor Cause NAFLD Associated With PCOS

Many animal models of PCOS have been developed using prenatal, postnatal, or peripubertal androgen treatment (58-61). For our studies, we used a well-established (36, 37) PCOS mouse model involving subcutaneous implantation of a long-term (90-day) continuous slow-releasing DHT pellet in prepubertal (21-day-old) female mice to induce a PCOS phenotype. DHT (nonaromatizable) was used instead of testosterone to avoid any confounding effects arising from the aromatization of testosterone (estrogenic effects). The DHT pellet animals had 5× higher serum DHT levels (578.3 ± 22.8 vs 115.6 ± 12.5 pg/mL; enzyme-linked immunosorbent assay, Alpha Diagnostics International, assay sensitivity 6 pg/µL), were slightly overweight, had higher fasting (food deprived, water only for 24 hours), and fed blood glucose level (Accu-Chek glucometer, Roche) (Fig. 1A) compared to placebo animals at the end of the treatment (37). Moreover, similar to previous studies (59-60), our results in supplemental Fig. S1 show that all the DHT-treated animals were acyclic (52), developed cystic ovaries (52), and had significant hepatic steatosis (lipid and triglyceride accumulation) (Fig. 1A and B).

To determine the direct impact of androgens on liver steatosis, we created a hepARKO mouse model by crossing AR-floxed (38) with albumin-Cre mice and then inserted DHT pellets in these animals. The validation of the hepARKO is shown in the supplemental (Fig. S2) (52). The AR messenger RNA (mRNA) and protein levels were barely detectable in the livers of hepARKO animals compared to Wt and heterogenous littermates. Moreover, AR mRNA and protein levels were not altered in the ovary, demonstrating the tissue-specificity of the AR depletion in the liver. Results show that in hepARKO DHT pellet-treated animals, body weight, and fed

A.

	WT-placebo	WT-DHT	hepARKO-DHT	hepARKO-placebo
Body weight (gm)	21.75 ± 1.82	25.8 ± 1.63*	22.1 ± 1.4	21.55 ± 1.9
Blood glucose (fasting) mg/dL	110.6 ± 12.6	220.5 ± 10.2*	120.1 ± 15.2	112.8 ± 9.2
Blood glucose (fed) mg/dL	169.1 ± 18.2	463 ± 17.2*	187.6 ± 19.1	173.7 ± 12.6

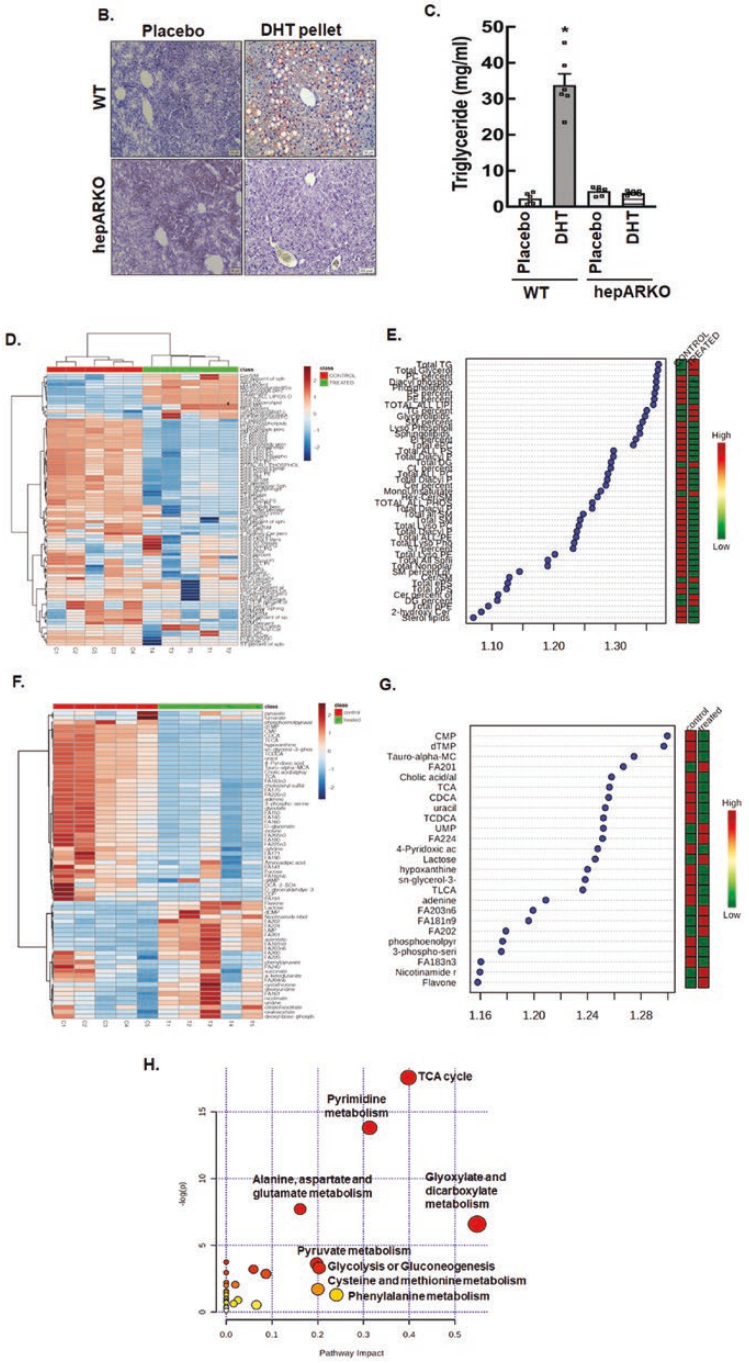

Figure 1. Chronic high levels of androgens significantly cause hepatic steatosis. (A) Metabolic features, (B) Oil Red O staining of liver sections, and (C) liver triglyceride levels isolated from wild-type (WT) and hepatocyte-specific androgen receptor knockout (hepARKO) mice after 90 days of placebo or dihydrotestosterone (DHT) pellet treatment. Data are the mean ± SE of the mean (n = 6 mice/treatment group). $^*P \leq 0.01$ vs placebo using 1-way analysis of variance followed by Dunnett's multiple comparison test). (D) Hierarchical clustering shown as heatmap of lipid classes in livers isolated from placebo (control) or DHT (treated) pellet mice (n = 5 mice/treatment). (E) Important lipid classes identified by partial least squares-discriminant analysis (PLS-DA) and represented as the average of the variable importance in projection (VIP) scores. The boxes on the right indicate the relative concentrations of the corresponding lipid class in each group (placebo-control vs DHT-treated) (F) Hierarchical clustering shown as heatmap of metabolites isolated from livers of placebo (control) or DHT (treated) pellet mice (n = 5 mice/treatment). (G) Important metabolites identified by PLS-DA and represented as the average of the VIP scores. The boxes on the right indicate the relative concentrations of the corresponding metabolites in each group (placebo control vs DHT-treated). (H) Graphical presentation of metabolome pathways in the liver impacted by DHT pellet treatment.

and fasting blood glucose levels, as well as hepatic steatosis phenotype, are completely rescued (Fig. 1A-1C) compared to DHT pellet-treated mice. Without DHT treatment (and under normal chow), hepARKO-placebo mice were similar to Wt placebo animals (Figs. 1A-1C), which is in accordance with previous studies (62).

High Androgen Levels Alter the Hepatic Metabolomic Milieu

Metabolomic studies (LC-MS) in liver samples from DHT and placebo pellet-treated animals reveal a significant increase in liver triglyceride and total lipid content in the DHT pellet-treated animals. Figure 1D and 1F shows a heatmap representing hierarchical clustering of all significant lipids (Fig. 1D) and metabolites (Fig. 1F) in livers from placebo vs DHT pellet-treated animals. We analyzed the data by a supervised, multivariate classification technique [partial least squares-discriminant analysis (PLS-DA)] to separately assess the overall segregation of the samples for placebo and DHT pellet-treated livers. Based on the PLS-DA model for placebo and DHT pellet-treated samples, we extracted lipids and metabolites that contributed significantly to the differentiation between placebo and DHT pellet-treated livers by using variable importance in projection (VIP) scores as a quantitative estimation. VIP scores were extracted for components 1 and 2 that showed a clear separation between placebo and DHT pellet-treated samples [PLS-DA score plots shown in supplemental (Fig. S4) (52)]. Figure 1E and 1G represents VIP score plots of lipids and metabolites, respectively, from livers of DHT pellet (treated) and placebo (control) animals. Results show total all lipids, including monoglycerolipids, triglycerolipids, glycerolipid, and diglycerides, as well as total lysophosphatidylcholine, were significantly increased in livers isolated from DHT pellet-treated animals compared to placebo animals. In contrast, total ceramide-1-phosphate, e-phosphatidyl serine, total polar sphingolipids, total plasmalogen, sulfatide lipids, and total e-phosphatidylcholine were some key lipid classes that were significantly lower in DHT pellet-treated livers vs placebo. A list of lipid features and metabolites identified in DHT pellet-treated livers vs placebo by fold-change analysis is shown in the supplemental (Fig. S4) (52). Pathway analysis (Fig. 1H) of liver metabolites reveals that the citrate cycle, pyrimidine metabolism, amino acid (alanine, aspartate, and glutamate) metabolism, and glyoxylate and dicarboxylate metabolism to be the most affected metabolic pathways in the DHT pellet-treated livers compared to placebo. Detailed results of the pathway analysis are provided in the supplemental (Fig. S4) (52).

High Androgen Levels Alter Hepatic Transcriptome

To further understand the overall impact of androgen excess on liver function, we next performed an RNA-seq study in DHT-treated vs placebo control liver samples. DESeq2 analysis identified a total of 787 annotated significant Ensembl DEGs. Out of these genes, 361 were upregulated, and 426 were downregulated genes. Hierarchical clustering of all the significant DEGs in placebo vs DHT pellet-treated livers is shown in Figure 2A, while the global transcriptional change across the 2 groups compared (placebo vs DHT) is represented by a volcano plot in Figure 2B. The complete list of significant DEGs is presented in the supplemental (Fig. S1) (52). Based on established hepatic functions, 5 upregulated DEGs (*Kdm5c, Cidea, Cidec, Fgf21*, and *Pparγ*) and 2 downregulated DEGs (*Agxt* and *Hint2*) were selected for validation of the RNA-seq data by qRT-PCR. Figure 2C shows that mRNA abundance of *Kdm5c, Cidea*, *Cidec*, *Fgf21*, and *Pparγ* are significantly elevated while *Agxt* and *Hint2* were downregulated in livers isolated from DHT pellet-treated animals compared to placebo animals. Results show that some key metabolic genes known to be upregulated in NAFLD, such as *Cidea* and *Cidec* (cell death-inducing DFFA like effector A and C; involved in lipid storage and formation of large lipid droplets) (63), (Fig. 2C), *Pparγ* (proliferator-activated receptor gamma; nuclear receptor) (64) (Fig. 2C), *Fgf21* (fibroblast growth factor 21; regulator of carbohydrate and lipid metabolism) (65, 66) (Fig. 2C), *Chka* (choline kinase alpha; plays a key role in phospholipid biosynthesis) (Fig. 2C), *Plin2* (perilin-2; encodes lipid droplet protein used as a marker of lipid droplets) (67), and *Mogat1* (monoacylglycerol acyltransferase; contributes to hepatic glyceride pools) (68, 69) are upregulated in the livers of DHT pellet animals compared to placebo. In contrast, genes such as *Agxt* (alanine-glyoxylate aminotransferase; breakdown of fats and removing toxic substances) (70, 71) (Fig. 2C), *Hint2* (histidine triad nucleotide binding protein 2; involved in mitochondrial function) (72) (Fig. 2C), and *Prdx4* (peroxiredoxin; protects against oxidative damage) (73) known to be decreased in NAFLD are downregulated in the livers of DHT pellet-treated animals compared to placebo (Fig. 2G). Notably, the expression of *Kdm5c*, *Cidea*, *Cidec*, *Fgf21*, *Pparγ*, *Agxt*, *Hint2*, *Chka*, *Ppp1r3c*, *Plin2*, *Adcy6*, and *Mogat1* were not upregulated in the livers from hepARKO-DHT mice (Fig. 2C). The expression of these genes in livers isolated for hepARKO-placebo mice were similar to placebo pellet-treated animals. This suggests that while androgens are not essential for expression of hepatic genes in females, under hyperandrogenic conditions, the expression of these genes are upregulated by androgens in the liver. In silico analysis revealed that a large number of the DEGs have ≥1 AR element (ARE) sequences in the promoter and/or distal (within 1 Kb) region, thereby suggesting that most of these genes are regulated directly by AR, rather than secondary effects of hormone exposure. To further verify that AR, through direct ARE binding, regulates the expression of these genes, ChIP-qPCR studies with AR antibody were performed. Results show that DHT treatment increases AR binding to AREs located on the promoter region of the previously mentioned genes and is significantly lower in hepARKO animals (Fig. 2D).

Biological pathway analysis (Fig. 2E) revealed genes of different categories and pathways were altered in livers isolated from DHT pellet-treated mice compared to placebo. Metabolic process, cell proliferation, and immune system process in the liver were some of the key pathways primarily affected by high androgen levels. Given that the metabolic process was the single largest biological pathway affected by hyperandrogenism, we focused our studies on these metabolic genes to gain further insight into androgen actions in the liver. Our studies show that out of the total 787 DEGs, 236 were metabolic genes, out of which 103 were upregulated and 133 were downregulated. Figure 2F represents the hierarchical clustering of all the significant metabolic DEGs in placebo vs DHT pellet-treated livers, and the top 12 up- and downregulated metabolic genes are shown in Figure 2G. Biological pathway analysis by gene ontology of the metabolic genes (supplemental Fig. S3) shows that lipid storage and its regulation, fat

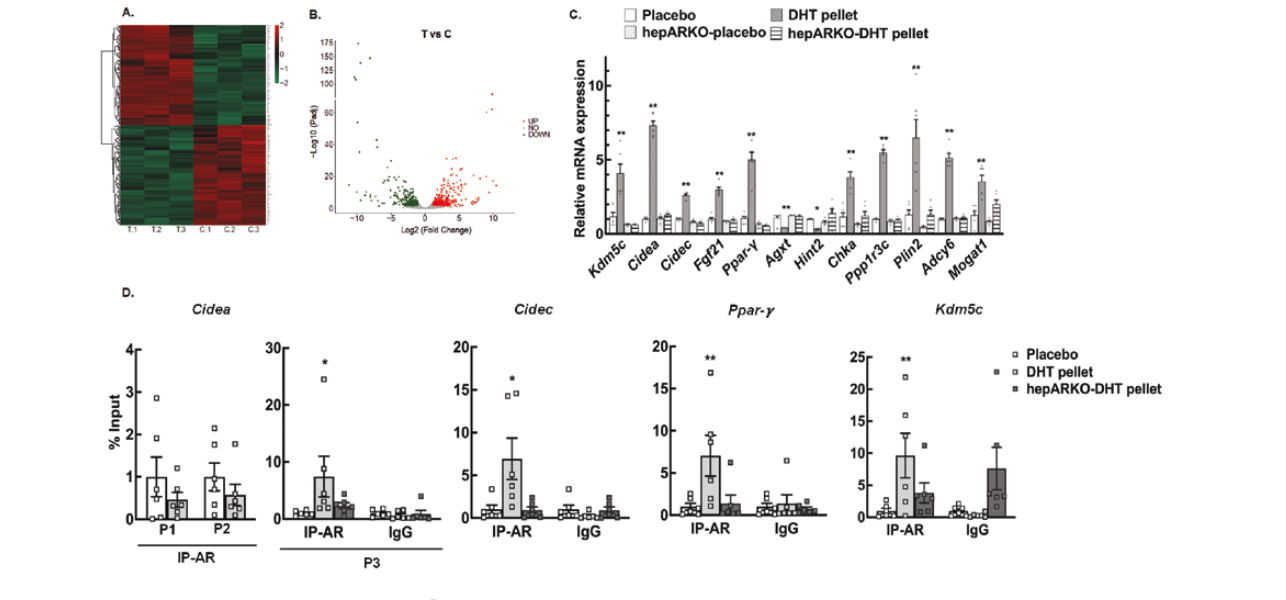

Top 12 up regulated metabolic genes out of 103	Log_2 fold change	Adjusted *p*-value
Kdm5c	10.4329698	3.24E-15
Cyp4a12a	8.97916714	4.83E-61
Cidea	7.81709462	2.24E-07
Elovl3	5.87853965	5.17E-16
Cidec	5.14905359	1.67E-18
Mtnr1a	5.09364179	8.16E-25
Mup20	4.89413442	4.24E-13
Mogat1	4.39346852	7.43E-11
Nat8	4.23305209	4.56E-14
Fgf21	4.15522166	2.61E-16
Lrp2	3.91177927	2.99E-05
Cyp2d9	3.78988243	1.29E-21

Top 12 down regulated metabolic genes out of 133	Log_2 fold change	Adjusted *p*-value
Agxt	-1.2475688	0.01590721
Afmid	-1.2289489	0.04625912
Prdx4	-1.2077511	0.0361639
Tgfbr3	-1.2007359	0.01825085
Wnt5b	-1.15426	0.03795475
Casp3	-1.1432472	0.02444867
Gsto1	-1.1159261	0.00016907
Hint2	-1.1006743	0.02650166
Gne	-1.0991636	0.02056214
Odc1	-1.0599979	0.00074444
Lbr	-1.0597769	0.00245094
Igf1	-1.0397319	0.00066898

Figure 2. High level of androgen changes the hepatic transcriptomic profile. (A) Hierarchical clustering is shown as a heatmap of differentially expressed sorted by adjusted *P*-value by plotting their log2 transformed expression values in samples (n = 3 mice/treatment). (B) Volcano plot representing the global transcriptional change across the groups compared. Each data point in the scatter plot represents a gene. Genes with an adjusted $P \leq 0.05$ and a log2 fold change ≥ 1 are indicated by red dots and represent upregulated genes. Genes with an adjusted $P \leq 0.05$ and a log2 fold change ≤ -1 are indicated by green dots and represent downregulated genes. (C) Relative expression of *Kdm5c* (lysine-specific demethylase 5C), *Cidea, Cidec* (cell death-inducing DFFA-like effector A and C), *Fgf21* (fibroblast growth factor 21), *Pparγ* (proliferator-activated receptor gamma), *Agxt* (alanine-glyoxylate aminotransferase), and *Hint2* (histidine triad nucleotide binding protein 2) and metabolic genes *Chka* (choline kinase alpha), *Ppp1r3c* (protein phosphatase 1 regulatory subunit 3C), *Plin2* (perilipin 2), *Adcy6* (adenylate cyclase 6), and *Mogat1* (monoacylglycerol O-acyltransferase 1) messenger RNA levels by quantitative real-time polymerase chain reaction in livers isolated from wild-type placebo and dihydrotestosterone (DHT) pellet-treated mice as well as hepatocyte-specific androgen receptor knockout (hepARKO) mice treated with placebo or DHT pellets. Data are displayed as means ± SE of the mean (n = 6 mice/treatment) and normalized to *Rpl19*. $*P \leq 0.05$, $**P \leq 0.01$ vs placebo using 1-way analysis of variance followed by Dunnett's multiple comparison test). (D) Anti-AR chromatin immunoprecipitation assay in livers isolated from wild-type placebo and DHT pellet-treated mice as well as hepatocyte-specific AR knockout (hepARKO) mice treated with DHT-pellet, showing AR binding to different AR element sequences on *Cidea* [P1: −289 bp, P2:−119 bp, and P3: 4 bp from transcription start site (TSS)], *Cidec* (−102 bp from TSS), *Pparγ* (−463 bp from TSS) and *Kdm5c* (−744 bp from TSS) promoter region. Immunoglobulin G (IgG) represents a nonspecific antibody. Values represent percentage input. Data are displayed as mean ± SE of the mean (n = 6 mice/treatment). $*P \leq 0.05$ for P3 *Cidea* and *Cidec*, $**P \leq 0.01$ for *Kdm5c* and *Pparγ* vs placebo using Student's *t*-test (E) Gene ontology analysis of enriched pathways in the differentially expressed gene sets. (F) Hierarchical clustering is shown as a heatmap of differentially expressed metabolic genes sorted by adjusted p-value by plotting their log2 transformed expression values in samples (n = 3 mice/treatment). (G) List of top 12 up- and downregulated metabolic genes.

cell differentiation, and fatty acid metabolic process are some of the key biological processes affected in the liver by the 103 upregulated metabolic genes (52). In contrast, epoxygenase P450 pathway, eicosanoid metabolic process, and unsaturated fatty acid metabolic process are the top pathways affected by the upregulated metabolic genes (52).

High Androgen Levels Associated With PCOS Affect a Number of Hepatic Circadian Genes

Interestingly, 240 circadian genes were also differentially regulated (127 upregulated and 113 downregulated) in the livers of DHT pellet-treated mice compared to placebo. The circadian clock is an endogenous timing system that drives numerous physiological processes (74). The circadian timing system is a key regulator of liver metabolism as hepatic health is maintained by proper timing of metabolic gene expression (75-77). In humans, variations in transcription factors involved in circadian rhythms are associated with NAFLD susceptibility and progression (78). The molecular clock is an autoregulatory transcription based feedback loop oscillator consisting of a group of transcriptional regulators referred to collectively as clock genes (79). The core loop (Fig. 3A) includes the transcriptional activator, *brain and muscle arntl-like1* (BMAL1) and its binding partner CLOCK, a histone acetyltransferase

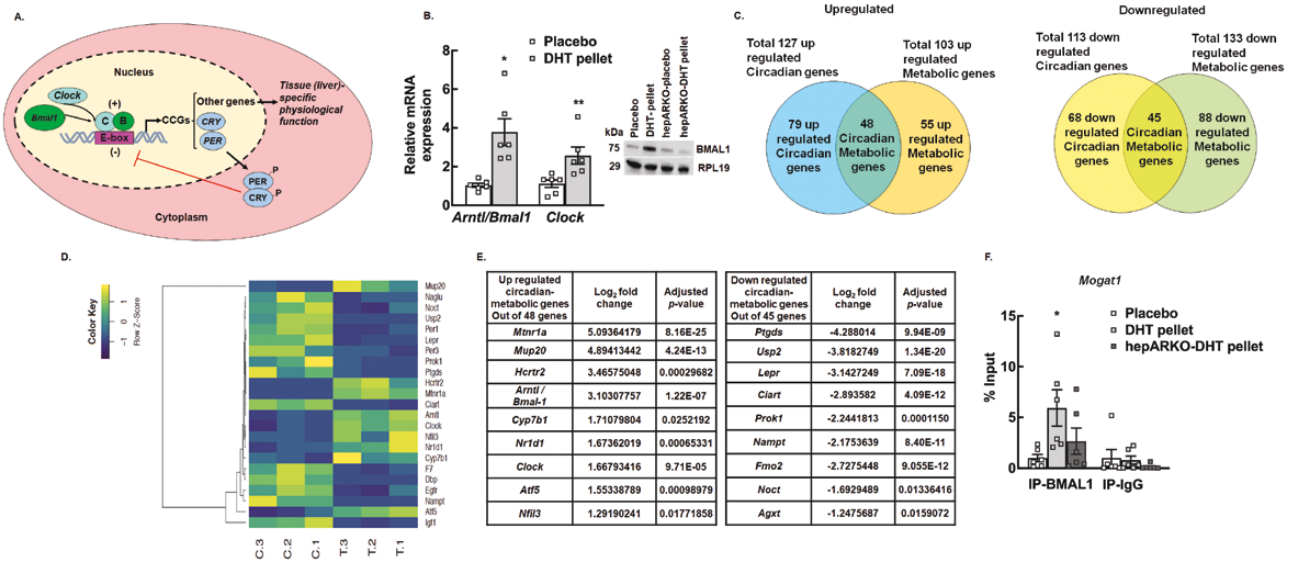

Up regulated circadian-metabolic genes Out of 48 genes	Log_2 fold change	Adjusted *p*-value
Mtnr1a	5.09364179	8.16E-25
Mup20	4.89413442	4.24E-13
Hcrtr2	3.46575048	0.00029682
Arntl / Bmal-1	3.10307757	1.22E-07
Cyp7b1	1.71079804	0.0252192
Nr1d1	1.67362019	0.00065331
Clock	1.66793416	9.71E-05
Atf5	1.55338789	0.00098979
Nfil3	1.29190241	0.01771858

Down regulated circadian-metabolic genes Out of 45 genes	Log_2 fold change	Adjusted *p*-value
Ptgds	-4.288014	9.94E-09
Usp2	-3.8182749	1.34E-20
Lepr	-3.1427249	7.09E-18
Ciart	-2.893582	4.09E-12
Prok1	-2.2441813	0.0001150
Nampt	-2.1753639	8.40E-11
Fmo2	-2.7275448	9.055E-12
Noct	-1.6929489	0.01336416
Agxt	-1.2475687	0.0159072

Figure 3. High level of androgen affects the expression of a large number of hepatic circadian genes important for liver metabolism. (A) Schematic of the molecular clock. (B) Relative expression of core clock genes, *Arntl1/ Bmal1* (brain and muscle arntl-like 1) and *Clock* (clock circadian regulator) messenger RNA levels by quantitative real-time polymerase chain reaction in livers isolated from wild-type placebo and dihydrotestosterone (DHT) pellet-treated mice. Data are displayed as means ± SE of the mean (n = 6 mice/ treatment) and normalized to *Rpl19*.* $P \leq 0.01$ for *Arntl/Bmal1*, ** $P \leq 0.05$ for *Clock* vs placebo using Student's *t*-test. Representative immunoblots (inset) showing total protein levels of BMAL1 in liver samples isolated from wild-type mice treated with placebo pellet, DHT pellet, and hepatocyte-specific androgen receptor (AR) knockout mice treated with placebo or DHT pellet. RPL19 protein level was used as internal control. (C) The total number of up- and downregulated metabolic genes regulated by the hepatic circadian clock was identified by comparing the total number of differentially regulated circadian and metabolic genes. (D) Hierarchical clustering is shown as a heatmap of differentially expressed circadian metabolic genes sorted by adjusted *P*-value by plotting their log2 transformed expression values in samples (n = 3 mice/treatment). (E) List of top 9 up- and downregulated circadian-metabolic genes. (F) Anti-BMAL1 chromatin immunoprecipitation assay in livers isolated from wild-type placebo and DHT pellet-treated mice as well as hepatocyte-specific AR knockout (hepARKO) mice treated with DHT pellet, showing BMAL1 binding on Mogat1 promoter region (−104 bp from transcription start site). Immunoglobin G (IgG) represents a nonspecific antibody. Values represent percentage input. Data are displayed as mean ± SE of the mean (n = 6 mice/treatment). * $P \leq 0.05$ vs placebo using 1-way analysis of variance followed by Dunnett's multiple comparison test.

that drives the expression of several genes, including the repressors *Period* (*Per1*, *Per2*, *Per3*) and *Cryptochrome* (*Cry1*, *Cry2*). PER and CRY in a negative feedback loop act as potent repressors of BMAL1:CLOCK-dependent transcription (Fig. 3A). BMAL1:CLOCK and PER:CRY are considered the core clock genes. Our results show that the mRNA expression of both *Bmal1* (*Arntl*) and *Clock* (Fig. 3B) as well as protein level of BMAL1 (Fig. 3B, inset) are significantly elevated in livers from DHT pellet-treated animals compared to placebo mice, and AR ablation in DHT pellet-treated animals restore BMAL1 protein to placebo levels (Fig. 3B, inset). In addition to the core clock genes, the BMAL1L:CLOCK complex also drives the rhythmic expression of a multitude of cell-specific genes, collectively termed "clock-controlled genes" (Fig. 3A) that underlie rhythms of cellular activity. In the liver, there are several clock-controlled genes that are critical to normal liver function (80). Therefore, to understand the effect of androgen-induced changes of clock-controlled hepatic gene expression on liver metabolism, we compared the differentially expressed circadian genes to metabolic genes. Results show that there were 48 upregulated and 45 downregulated clock-controlled metabolic genes in DHT pellet-treated livers compared to placebo (Fig. 3C). Figure 3D represents the hierarchical clustering of all the clock-controlled metabolic DEGs in placebo vs DHT pellet-treated livers; the top up- and downregulated clock-controlled metabolic genes are shown in Figure 3E.

Based on these studies, we hypothesized that in the liver, high androgen levels associated with PCOS increase the expression of *Bmal1* and *Clock*, which in turn induces the expression of different metabolic genes resulting in hepatic steatosis. To prove this hypothesis, we performed ChIP-qPCR with BMAL1 antibody on the promoter region of *Mogat1* (BMAL1 binding site determined by in silico analysis). Results show significant BMAL1 binding on the promoter region of *Mogat1* under hyperandrogenic conditions compared to control (placebo-treated), which is reversed with liver-specific ablation of AR (Fig. 3F).

High Androgen Levels Associated With PCOS Disrupt the Circadian Timing-System in the Liver Through Epigenetic Modifications

To determine the effect of high androgen levels on the hepatic clock, we developed a DHT pellet-induced PCOS mouse model using a well-established knock-in mouse (Jackson Lab) that expresses a PER2::LUC fusion protein, allowing for real-time ex vivo monitoring of molecular clock function. Liver tissue from DHT and placebo pellet-treated animals were collected, and bioluminescence was continuously recorded (counts per second) with an automated luminometer as described in the Materials and Methods section (55). Figure 4A shows representative traces of PER2::LUC expression in liver explants from DHT and placebo pellet-treated mice. Results show that chronic high androgen level disrupts the circadian timing system in the liver. DHT pellet-treated liver samples showed high amplitude (Fig. 4B), but there was not a significant phase shift (Fig. 4C) between DHT and placebo pellet-treated livers with respect to the peak expression of PER2::LUC.

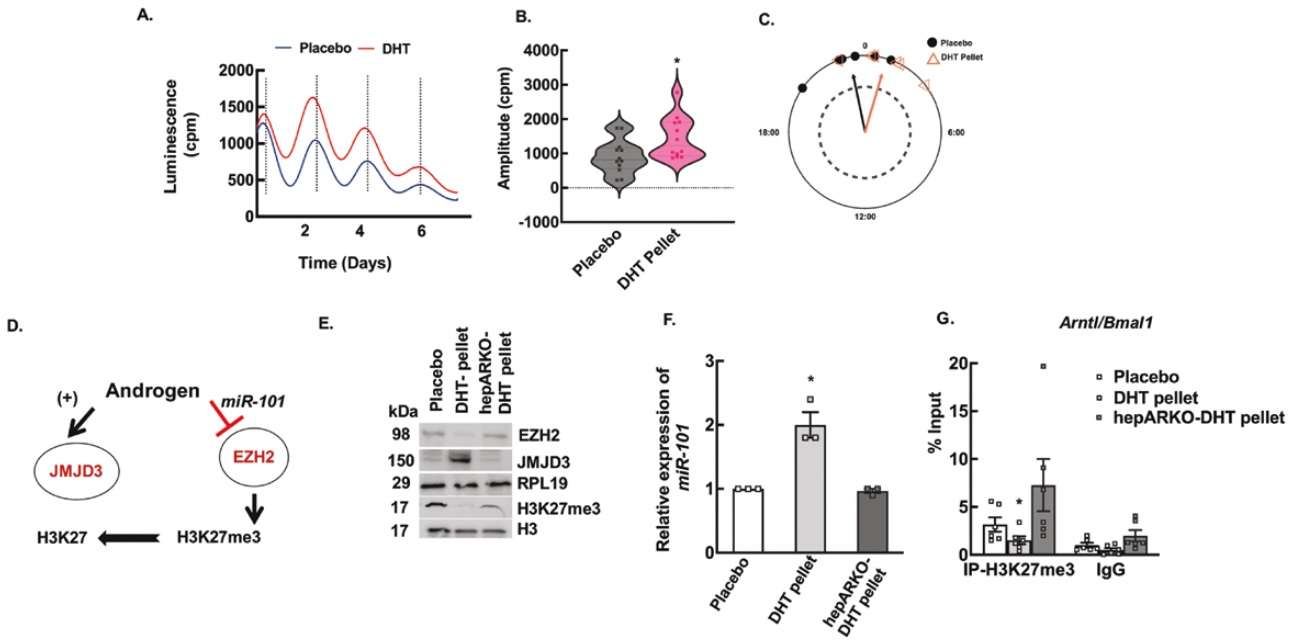

Figure 4. Elevated androgen levels disrupt the circadian timing system in the liver through epigenetic modulation. (A) Representative traces of Period2::Luciferase (PER2::LUC) expression in liver explants from dihydrotestosterone (DHT) and placebo pellet mice. The peak of the tissue from DHT-pellet animals peaks slightly earlier than the placebo pellet-treated mice, indicating that DHT reduces the peak-to-peak time, thus advancing the overall peak of PER2 expression over 5 days. (B) The amplitude of the first 2 peaks of PER2::Luc luminescence was calculated by LM fit (damped sine) method (LumiCycle analysis, Actimetrics) from liver tissues isolated from placebo and DHT pellet-treated mice. Data are displayed as mean ± SE of the mean (n = 6 mice/ treatment). $*P \leq 0.05$ vs placebo using Student's *t*-test. (C) The time of day of the first PER2::LUC peak was used to establish the phase of the studied tissue. Phase relationship is represented in radians with circular mean deviation. The mean of the first peak is indicated by the vector lines and symbols indicate individual data points. Rayleigh test of uniformity revealed clustering of the studied tissues, indicated by arrowheads crossing the dotted circle ($P = 0.05$). (D) Schematic showing androgen-induced regulation of H3K27me3 mark. (E) Representative immunoblots showing total protein levels of EZH2, JMJD3, and H3K27me3 in liver samples isolated from wild-type mice treated with placebo pellet, DHT pellet, and hepatocyte-specific androgen receptor knockout (hepARKO) mice treated with DHT pellet. RPL19 and H3 protein levels are used as internal controls. (F) Relative expression of *miR-101* by quantitative real-time polymerase chain reaction in livers isolated from wild-type mice treated with placebo pellet, DHT pellet, and hepARKO mice treated with DHT pellet. Data are displayed as means ± SE of the mean (n = 3 mice/ treatment) and normalized to *snoRNA202*. $*P \leq 0.01$ vs placebo using Student's *t*-test. (G) Anti-H3K27me3 chromatin immunoprecipitation assay in livers isolated from wild-type placebo and DHT pellet-treated mice as well as hepARKO mice treated with DHT pellet, showing H3K27me3 enrichment on *Arntl* (*Bmal1*) promoter region (within 500 bp from transcription start site). Immunoglobin G (IgG) represents a nonspecific antibody. Values represent percentage input. Data are displayed as mean ± SE of the mean (n = 6 mice/treatment). $*P \leq 0.05$ vs placebo using 1-way analysis of variance followed by Dunnett's multiple comparison test.

Both placebo (0.21820 rad ± 0.327; Rayleigh = 0.9174, $P = 0.0019$) and DHT pellet-treated (–0.28360 rad ± 0.327; Rayleigh = 0.9252, $P = 0.0016$) livers exhibited a significant mean direction for their phase (Watson's 2-sample test of homogeneity = 0.0764, $P > 0.10$).

To determine whether the expression of *Bmal1* (*Arntl*) is directly regulated by androgens through AR-ARE interaction, we initially scanned in silico for AREs on the *Bmal1* (*Arntl*) promoter region that revealed 1 ARE binding site (Fig. S5) (–592 from TSS). However, ChIP-qPCR studies show no AR binding to this ARE site on the *Bmal1* promoter in liver samples isolated from DHT pellet-treated mice compared to placebo pellet-treated mice (52). Previous studies from our laboratory have reported that in addition to regulating gene expression through AR-ARE interaction, androgens can also regulate/influence the expression of genes via epigenetic modulation. Our studies in the ovary (33, 34) show that H3K27me3 (trimethylation of lysine 27 on histone 3), which is a gene repressive mark, is a downstream target of androgen actions. We have reported that androgen-induced decrease of H3K27me3 is mediated through (1) inhibiting the expression and activity of enhancer of zeste homologue 2 (EZH2), a histone methyltransferase that promotes trimethylation of K27 through inducing the expression of a microRNA, *miR-101*, that targets *Ezh2* expression (33), and (2) by inducing the expression of a histone demethylase called Jumonji domain containing protein-3 (JMJD3/KDM6B) (34), responsible for removing the H3K27me3 mark (Fig. 4D). In our effort to elucidate the underlying mechanism of how androgens regulate *Bmal1* expression, we assessed androgen-induced modulation of H3K27me3 in liver samples isolated from DHT and placebo pellet-treated animals. Results show that under hyperandrogenic conditions, there was a significant decrease in H3K27me3 in mouse liver, while hepatic EZH2 levels were decreased and JMJD3 levels were elevated (Fig. 4E). The expression of *miR-101* was also upregulated in livers of DHT pellet-treated mice (Fig. 4F). Furthermore, ChIP-qPCR assays with H3K27me3 antibodies on the *Bmal1* promoter region show significantly lower H3K27me3 levels in liver samples isolated from DHT-pellet vs placebo animals (Fig. 4G). In contrast, these effects were completely reversed in hepARKO animals treated with DHT pellets (Fig. 4E-4G). These studies establish that *Bmal1* expression is regulated by androgen-induced decrease of H3K27me3.

To further demonstrate that androgens directly disrupt the hepatic circadian system, in vitro studies using liver

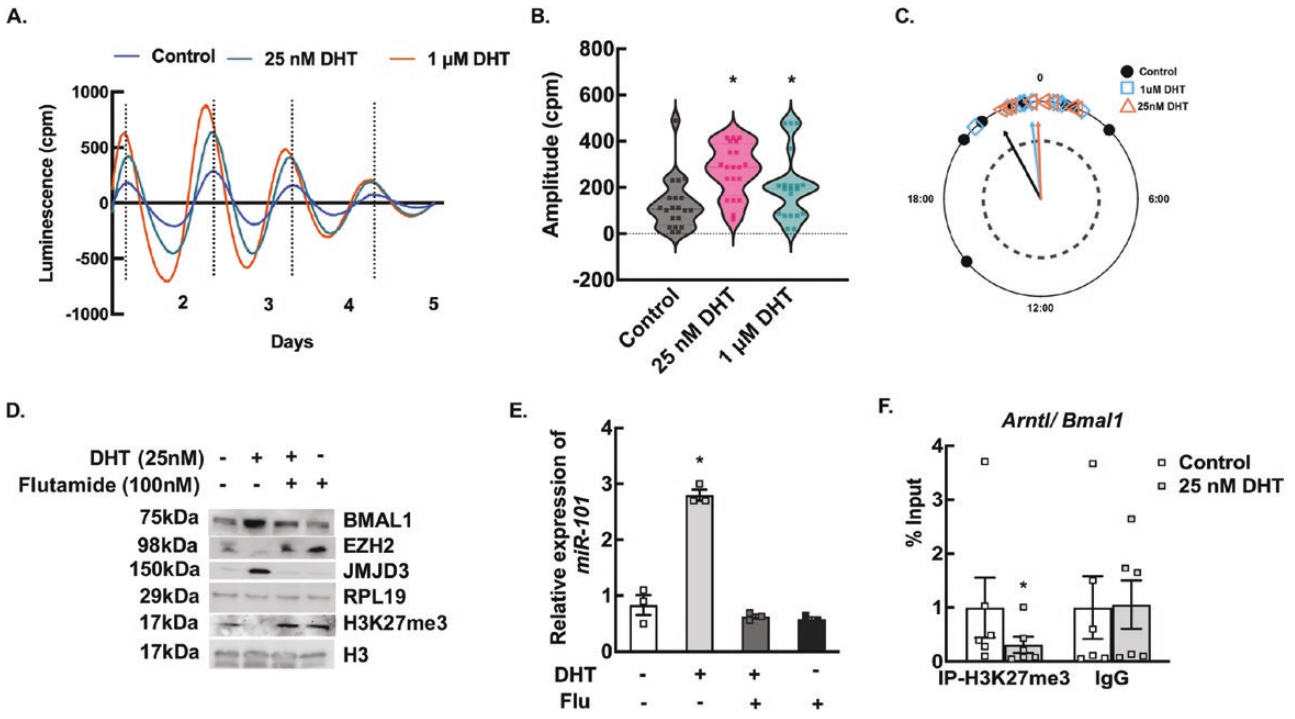

Figure 5. In vitro androgen treatment of liver tissues mimic in vivo effects with respect to disruption of the circadian timing system and epigenetic modulations. (A) Representative traces of Period2::Luciferase (PER2::LUC) expression in liver explants treated in vitro with vehicle only (control) and 25 nM and 1 μM of dihydrotestosterone (DHT) for 5 days. (B) The amplitude of the second peak of PER2::Luc luminescence was calculated by LM fit (damped sin) method (LumiCycle analysis, Actimetrics) from liver tissues treated in vitro with vehicle only (control) and 25 nM and 1 μM of DHT for 5 days. Data are displayed as mean ± SE of the mean (n = 20 samples/treatment). *$P \leq 0.01$ vs control using Student's *t*-test. (C) The time of day of the first PER2::LUC peak was used to establish the phase of the studied tissue. Phase relationship is represented in radians with circular mean deviation. The mean of the first peak is indicated by the vector lines and symbols indicate individual data points. Rayleigh test of uniformity revealed clustering of the studied tissues, indicated by arrowheads crossing the dotted circle ($P = 0.05$). (D) Representative immunoblots showing total protein levels of BMAL1, EZH2, JMJD3, and H3K27me3. Total protein levels of RPL19 and H3 were used as internal controls (E) Relative expression of *miR-101* by quantitative real-time polymerase chain reaction (RT-PCR) in liver samples treated (24 hours) in vitro with vehicle only (control) and 25 nM of DHT in presence or absence of flutamide (100 nM). RPL19 and H3 protein levels are used as internal controls for the immunoblots. For quantitative RT-PCR, data are displayed as means ± SE of the mean (n = 3 experiments/treatment) and normalized to *snoRNA202*. *$P \leq 0.01$ vs control using 1-way analysis of variance followed by Dunnett's multiple comparison test). (F) Anti-H3K27me3 chromatin immunoprecipitation assay in liver tissues treated (24 hours) in vitro with vehicle only (control) and 25nM of DHT, showing H3K27me3 enrichment on *Arntl* (*Bmal1*) promoter region (within 500 bp from transcription start site). Immunoglobin G (IgG) represents a nonspecific antibody. Values represent percentage input. Data are displayed as mean ± SE of the mean (n = 6 experiments/ treatment). *$P \leq 0.01$ vs control using Student's *t*-test.

explants isolated from PER2::LUC mice cultured with DHT (25 nM and 1 μM) or vehicle control were performed. For the in vitro studies, the amplitude and phase shift of PER2::LUC expression (Fig. 5A-5C) were significantly different between control and DHT treatment. For phase shift analysis (Fig. 5C), all groups passed the Rayleigh test of uniformity, with control (Rayleigh = 0.696, $P < 0.0001$), 1 μM (Rayleigh = 0.9413, $P < 0.0001$), and 25 nM (Rayleigh = 0.9659, $P < 0.0001$) all exhibiting a significant mean phase. The circular analysis of variance involving a high concentration F-test [$F(21,59) = Inf$, $P < 0.0001$] (81, 82) and subsequent post hoc Watson's 2-sample test of homogeneity revealed significant differences in the timing of the phase between the control (0.4977 rad ± 0.615) and both the 1 μM DHT treatment dose (0.1132 rad ± 0.273; Watson's = 0.2028, $0.01 < P < 0.05$) and the 25 nM DHT treatment dose (0.04071rad ± 0.223; Watson's = 0.3019, $0.001 < P < 0.01$). Moreover, similar to in vivo studies, in vitro treatment of liver tissues with 25 nM DHT (24 hours) caused a significant decrease in EZH2 and elevated JMJD3, resulting in lower H3K27me3 levels (Fig. 5D). Moreover, in accordance with in vivo studies (Fig. 3B, inset), in vitro studies also show that 25 nM of DHT treatment increases the BMAL1 protein levels (Fig. 5D), as well as upregulated the expression of *miR-101* (Fig. 5E). Flutamide, an AR inhibitor, blocked these DHT effects, thereby mimicking the results observed in the hepARKO-DHT animals. Furthermore, ChIP-qPCR assays with H3K27me3 antibodies on the *Bmal1* promoter region show significantly lower H3K27me3 levels in liver tissues treated with DHT (Fig. 5F).

High Androgen Levels Also Alter Key Hepatic Metabolic and Circadian-Metabolic Genes in a Nonhuman Primate PCOS Model

To determine whether the changes in hepatic gene expression by high androgen levels are conserved in primate species, we extended our findings from the mouse PCOS model to a rhesus monkey PCOS model (Fig. 6). Results show that chronically elevated androgen not only increases the expression of core clock genes, *Arntl/Bmal1* and *Clock*, but also the expression of several metabolic genes, such as *Ddit3* (DNA damage inducible transcript 3 encoding for C/EBP homologous protein), *Fgf21*, *Mogat1*, and *Pparγ*. In

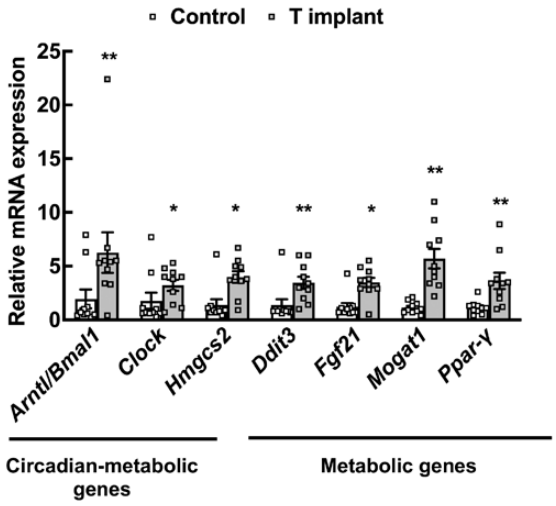

Figure 6. Expression of metabolic genes in livers of a nonhuman primate polycystic ovary syndrome model. Relative expression of *Arntl1/Bmal1* (brain and muscle arntl-like 1) and *Clock* (clock circadian regulator), *Hmgcs2* (3-hydroxy-3-methylglutaryl-CoA synthase 2), *Ddit3* (DNA damage inducible transcript 3), *Fgf21* (fibroblast growth factor 21), *Mogat1* (monoacylglycerol O-acyltransferase 1), and *Ppar-γ* (proliferator-activated receptor gamma) messenger RNA levels by quantitative real-time polymerase chain reaction in livers isolated from female rhesus macaques treated with control (cholesterol implants) or testosterone implants for 5 years. Data are displayed as means ± SE of the mean (n = 10 animals/ treatment) and normalized to *Rpl32*. $*P \leq 0.05$ for *Clock*, *Hmgcs2*, and *Fgf21*; $**P \leq 0.01$ for *Arntl/Bmal1*, *Ddit3*, *Mogat1*, and *Ppar-γ* vs control using Student's *t*-test.

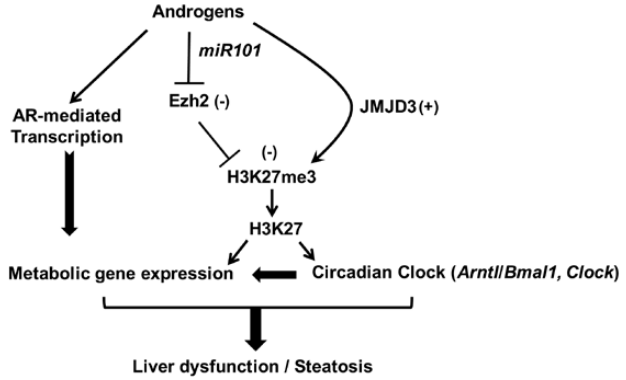

Figure 7. Proposed model of androgen-induced liver dysfunction leading to hepatic steatosis. Androgens decrease the H3K27me3, a gene-silencing mark on the promoter region of circadian clock genes like *Arntl/Bmal1* and *Clock,* which disrupts the circadian timing system. This is achieved by inhibiting the expression and activity of enhancer of zeste homologue 2 (EZH2), a histone methyltransferase that promotes trimethylation of K27 through inducing the face of a microRNA, *miR-101,* that targets *Ezh2* expression and by inducing the expression of a histone demethylase called Jumonji domain containing protein-3 (JMJD3/KDM6B), responsible for removing the H3K27me3 mark. These clock genes, in turn, regulate several metabolic genes. In addition, androgens also directly regulate the expression of several metabolic genes through the androgen receptor–mediated transcription in a clock-independent fashion. Both pathways lead to the development of hepatic steatosis in polycystic ovary syndrome mice.

addition, clock-controlled metabolic genes, such as *Hmgcs2* (3-hydroxy-3-methylglutaryl-CoA synthase 2), are also upregulated in livers isolated from PCOS rhesus monkeys (Fig. 6).

Discussion

This study highlights 3 major points (Fig. 7). First, direct androgen actions through the AR in the liver are a contributing factor to the hepatic steatosis seen in hyperandrogenic conditions associated with PCOS. Second, it provides an overall understanding of all the hepatic genes and metabolic pathways affected by high androgen levels. Third, in addition to direct regulation of gene expression through AR-ARE interaction, high androgen levels through epigenetic modification alter the circadian timing system in the liver that, in turn, negatively affects the expression of a number of metabolic genes (Fig. 7).

The PCOS patient population not only is highly heterogeneous, consisting of lean and obese PCOS patients, but also the range of elevated androgen level in this population significantly varies (83-86). To mimic this heterogeneity, different concentrations of DHT have been used to develop diverse murine models of hyperandrogenism associated with PCOS that manifests to various degrees of obesity and metabolic dysfunctions (61). The murine model developed with low doses of DHT (achieving 2-fold higher serum DHT levels) represents the lean PCOS phenotype and shows impaired glucose intolerance but no liver steatosis or obesity (87, 88). Studies in this model have reported that DHT-induced hepatocyte insulin resistance is driven by androgen-induced impaired liver metabolism and is reversed by the AR antagonist, flutamide (88) as well as deletion of hepatic AR (87). The DHT dose (2.5 mg) used to develop the murine PCOS model in this study achieves about a 5-fold increase in serum DHT levels, and the animals are slightly overweight, are glucose intolerant, and have liver steatosis. Also, in our model, deletion of hepatic AR rescues the liver steatosis phenotype. Similarly, animals in murine PCOS models with a very high DHT concentration (10 mg) develop obesity, glucose intolerance, and NAFLD, but studies in these animals show that adipose and brain-specific knockout of the AR could rescue these phenotypes (89). Based on these studies, it can be postulated that under low to medium hyperandrogenism, liver dysfunction (hepatic insulin resistance and hepatic steatosis) is primarily regulated through the hepatic ARs. In contrast, when androgen levels are very high, the adipose and brain-specific ARs are the primary driver of liver steatosis.

Additionally, this study provides an overall view of how hyperandrogenism affects liver metabolism. Our metabolomics and RNA-seq studies reveal that high androgen levels in general increase the synthesis of cholesterol and lipids in the liver, which is mediated by the upregulation of genes involved in various lipid/fatty acid metabolic pathways. A number of these metabolic genes contain ARE sequences in the promoter region, demonstrating that androgens can directly regulate these genes, thereby influencing liver metabolism. For example, *Mogat1*, which is upregulated in DHT pellet-treated livers, encodes monoacylglycerol acyltransferase that catalyzes the formation of diacylglycerol from 2-monoacylglycerol and fatty acyl-CoA and is the precursor of lipids such as triacylglycerol and phospholipids. Similarly, other upregulated genes, such as *Chka*, encoding for choline kinase alpha are involved in the biosynthesis of phosphatidylcholine via the cytidine diphosphate-choline pathway; *Osbp18*, encoding oxysterol binding protein-like 8 is involved in glycerophospholipid biosynthesis and phospholipid metabolism; and *Ddhd2*, encoding for a phospholipase enzyme

containing sterile-alpha motif, WWE, and DDHD domains, are involved in glycerophospholipid biosynthesis. These gene expression profiles correlate with our metabolomic data that show a high level of diacylglycerol as well as triacylglycerol, glycerophospholipid, and phospholipids in livers from DHT pellet-treated animals compared to placebo. Generally, fat accumulation arises from an imbalance between hepatic lipid uptake, de novo lipogenesis, and oxidation. Our RNA-seq data show increased expression of *Elovl3*, a gene encoding for elongation of very long-chain fatty acids protein 3 involved in de novo lipogenesis. Notably, livers of DHT pellet-treated animals also have increased expression of *Pparγ*, which is known to be involved in NAFLD (64) and has been reported to be high in liver steatosis (90). PPARγ regulates the expression of a number of fatty acid transporters (91), one of which is fatty acid translocase (CD36/FAT) encoded by *Cd36*, which is also upregulated in the DHT pellet-treated livers.

In contrast, our data suggest that a high level of androgen disrupts catabolism of hepatic fatty acids resulting in fat accumulation. This is reflected by the downregulation of a number of genes involved in fatty acid β oxidation [*Abcd2* (ATP-binding cassette sub-family D member 2), *Eci3* (enoyl-CoA delta isomerase 3), and Hsd17β4 (peroxisomal multifunctional enzyme type 2)] in livers of DHT pellet-treated animals. While AR is primarily seen as a transcription activator, AR can also act as a transcriptional inhibitor when it binds to DNA at enhancers and/or promoters by assembling repressive complexes involving histone/DNA deacetylases and methylases (92). Moreover, androgens can also induce transcription inhibitors, which, in turn, cause repression of genes. Another key gene that is upregulated in the DHT pellet-treated livers is *Fgf21,* which has a large number of metabolic functions (93) and is used as a biomarker and a therapeutic target of NAFLD (66, 94). Taken together, our transcriptomic and metabolomic data suggest that in females chronic hyperandrogenemia causes the accumulation of hepatic fat by stimulating de novo lipogenesis and increasing free fatty acid uptake and catabolism, as well as overall hepatic lipid biosynthesis.

In addition to AR-ARE–mediated regulation of gene expression, we find that high androgen levels can also indirectly influence hepatic gene expression through modulation of the hepatic circadian timing system. Emerging evidence suggests that PCOS women have circadian rhythm dysfunction and poorer sleep than non-PCOS women (95-98). A recent study in 436 PCOS patients and 715 control subjects reported a significant association between circadian rhythm disruption and PCOS (99). Circadian rhythms are near–24-hour patterns of physiology and behavior that are regulated by a master circadian pacemaker located in the suprachiasmatic nucleus (SCN) of the hypothalamus (100). Daily oscillations of light and darkness synchronize, or entrain, the circadian SCN pacemaker to the 24-hour day. Tissues outside the SCN also have tissue-specific circadian clock (called "peripheral cellular clock") that influence tissue-specific functions and can be synchronized by circadian-driven behaviors such as feeding-fasting cycles (101). The circadian timing system has been associated with a large number of physiological (reproductive, metabolic, neuroendocrine) and pathophysiological conditions (102-105). It is believed that the disruption of the circadian system due to hyperandrogenemia is an underlying cause for the manifestation of various PCOS phenotypes (106, 107). In the liver (108), there are several clock-controlled genes (82, 109-111) that contribute to the daily rhythms of metabolism (112). Mutation or genetic deletion of a number of the core clock genes results in impaired expression of these metabolic genes leading to metabolic dysfunction, including NAFLD (113). Moreover, previous studies have reported that DHT pellet treatment-induced hyperandrogenism disrupts the circadian timing system in the PCOS mouse model (114). Our results are in accordance with these previous observations and provide direct evidence of androgen-induced disruption of the hepatic clock, as well as identify the disrupted clock-controlled metabolic genes in the PCOS liver.

Furthermore, this study offers a mechanistic understanding of how high androgen levels disrupt the hepatic circadian system. The studies in the liver reported here, along with our recent observations in the ovary (33, 34, 115), clearly show that H3K27me3 is a downstream target of androgen actions, and the decrease of this gene silencing mark through androgen-induced regulation of Ezh2, and Jmjd3 is conserved across tissues. Classically, ARs transcriptionally regulate gene expression by directly binding to AREs on the promoter region of the target genes. Our studies highlight that androgen-induced modulation of the H3K27me3 mark is another avenue, independent of AR-ARE actions, through which androgens can influence gene expression. While our results show that decreased levels of the H3K27me3 mark in the vicinity of the *Bmal1* promoter enables the increased transcription of *Bmal1,* implicating it in the disruption of the hepatic clock, the far-reaching impact of decreased H3K27me3 levels on overall hepatic gene expression and liver metabolism cannot be discounted. For example, expression of *Fgf21* and *Cidea*, 2 important metabolic genes upregulated in the DHT pellet-treated livers, are regulated by an Ezh2-Jmjd3–mediated decrease of H3K27me3 in glioblastoma stem cells (116) and adipocytes (117), respectively. Interestingly, downregulation of Ezh2 and the H3K27me3 mark is also associated with hepatic steatosis, NAFLD, and liver dysfunction (118).

The fact that the livers of both PCOS mice and nonhuman primate models have the same elevated circadian and metabolic genes in the liver not only demonstrates that the effects of chronic high androgen levels on hepatic gene expression are conserved but also strengthens the concept that direct androgen actions in the liver may be an underlying mechanism for liver dysfunction associated with PCOS. Interestingly, recent studies (56, 57) in the nonhuman primate PCOS model have reported no significant difference in the metabolic phenotype associated with PCOS between control and testosterone-treated groups. However, these studies included only body weight/body composition measurements, glucose tolerance, and insulin sensitivity determination (56, 57). As mentioned in the introduction, hepatic steatosis in PCOS can occur independent of obesity, and while NAFLD can be detected by computed tomography/magnetic resonance imaging, liver biopsy is the gold standard for diagnosing NAFLD. The gene expression data from the liver biopsies of nonhuman primate models presented here form the premise for a further in-depth investigation into the liver functions of these testosterone-treated animals.

In summary, our findings provide insight into the effect and underlying mechanism of high androgen associated with PCOS on female liver metabolism and highlight the hepatic genes and metabolic pathways associated with NAFLD in PCOS.

Funding

National Institute of Health R01HD086062, United State Department of Agriculture-HATCH project MICL02383, Michigan State University-General Funds and MSU AgBioResearch to A.S. and National Institute of Health R01GM131398, National Science Foundation DBI-1942143 to J.W. I.S. was partially supported by NIH (NICHD) under award no. T32HD087166. Nonhuman primate work was supported by the National Centers for Translational Research in Reproduction grant P50 HD071836 (NIH/NICHD) and Human Development and the Oregon National Primate Research Center grant P51 OD011092 from the NIH/Office of the Director.

Disclosures

The authors have nothing to disclose. The authors declare no conflict of interest.

Data Availability

All data generated or analyzed during this study are included in this published article or the data repositories listed in the references.

References

1. Bozdag G, Mumusoglu S, Zengin D, Karabulut E, Yildiz BO. The prevalence and phenotypic features of polycystic ovary syndrome: a systematic review and meta-analysis. *Hum Reprod*. 2016;31(12):2841-2855. doi:10.1093/humrep/dew218
2. Lizneva D, Suturina L, Walker W, Brakta S, Gavrilova-Jordan L, Azziz R. Criteria, prevalence, and phenotypes of polycystic ovary syndrome. *Fertil Steril*. 2016;106(1):6-15. doi:10.1016/j.fertnstert.2016.05.003
3. Kataoka J, Larsson I, Bjorkman S, Eliasson B, Schmidt J, Stener-Victorin E. Prevalence of polycystic ovary syndrome in women with severe obesity—effects of a structured weight loss programme. *Clin Endocrinol (Oxf)*. 2019;91(6):750-758. doi:10.1111/cen.14098
4. Teede H, Deeks A, Moran L. Polycystic ovary syndrome: a complex condition with psychological, reproductive and metabolic manifestations that impacts on health across the lifespan. *BMC Med*. 2010;8:41. doi:10.1186/1741-7015-8-41
5. Livadas S, Pappas C, Karachalios A, *et al*. Prevalence and impact of hyperandrogenemia in 1,218 women with polycystic ovary syndrome. *Endocrine*. 2014;47(2):631-638. doi:10.1007/s12020-014-0200-7
6. Legro RS, Driscoll D, Strauss JF 3rd, Fox J, Dunaif A. Evidence for a genetic basis for hyperandrogenemia in polycystic ovary syndrome. *Proc Natl Acad Sci USA*. 1998;95(25):14956-14960. doi:10.1073/pnas.95.25.14956
7. Moghetti P, Tosi F, Tosti A, *et al*. Comparison of spironolactone, flutamide, and finasteride efficacy in the treatment of hirsutism: a randomized, double blind, placebo-controlled trial. *J Clin Endocrinol Metab*. 2000;85(1):89-94. doi:10.1210/jcem.85.1.6245
8. Venturoli S, Marescalchi O, Colombo FM, *et al*. A prospective randomized trial comparing low dose flutamide, finasteride, ketoconazole, and cyproterone acetate-estrogen regimens in the treatment of hirsutism. *J Clin Endocrinol Metab*. 1999;84(4):1304-1310. doi:10.1210/jcem.84.4.5591
9. Calaf J, Lopez E, Millet A, *et al*; Spanish Working Group for Hirsutism. Long-term efficacy and tolerability of flutamide combined with oral contraception in moderate to severe hirsutism: a 12-month, double-blind, parallel clinical trial. *J Clin Endocrinol Metab*. 2007;92(9):3446-3452. doi:10.1210/jc.2006-2798
10. De Leo V, Lanzetta D, D'Antona D, la Marca A, Morgante G. Hormonal effects of flutamide in young women with polycystic ovary syndrome. *J Clin Endocrinol Metab*. 1998;83(1):99-102. doi:10.1210/jcem.83.1.4500
11. Paradisi R, Fabbri R, Battaglia C, Venturoli S. Ovulatory effects of flutamide in the polycystic ovary syndrome. *Gynecol Endocrinol*. 2013;29(4):391-395. doi:10.3109/09513590.2012.754876
12. Caldwell ASL, Edwards MC, Desai R, *et al*. Neuroendocrine androgen action is a key extraovarian mediator in the development of polycystic ovary syndrome. *Proc Natl Acad Sci USA*. 2017;114(16):E3334-E3343. doi:10.1073/pnas.1616467114
13. Caldwell AS, Eid S, Kay CR, *et al*. Haplosufficient genomic androgen receptor signaling is adequate to protect female mice from induction of polycystic ovary syndrome features by prenatal hyperandrogenization. *Endocrinology*. 2015;156(4):1441-1452. doi:10.1210/en.2014-1887
14. Dumesic DA, Oberfield SE, Stener-Victorin E, Marshall JC, Laven JS, Legro RS. Scientific statement on the diagnostic criteria, epidemiology, pathophysiology, and molecular genetics of polycystic ovary syndrome. *Endocr Rev*. 2015;36(5):487-525. doi:10.1210/er.2015-1018
15. Escobar-Morreale HF. Polycystic ovary syndrome: definition, aetiology, diagnosis and treatment. *Nat Rev Endocrinol*. 2018;14(5):270-284. doi:10.1038/nrendo.2018.24
16. Vassilatou E. Nonalcoholic fatty liver disease and polycystic ovary syndrome. *World J Gastroenterol*. 2014;20(26):8351-8363. doi:10.3748/wjg.v20.i26.8351
17. Kelley CE, Brown AJ, Diehl AM, Setji TL. Review of nonalcoholic fatty liver disease in women with polycystic ovary syndrome. *World J Gastroenterol*. 2014;20(39):14172-14184. doi:10.3748/wjg.v20.i39.14172
18. Asfari MM, Sarmini MT, Baidoun F, *et al*. Association of nonalcoholic fatty liver disease and polycystic ovarian syndrome. *BMJ Open Gastroenterol*. 2020;7(1):e000352. doi:10.1136/bmjgast-2019-000352
19. Kim JJ, Kim D, Yim JY, *et al*. Polycystic ovary syndrome with hyperandrogenism as a risk factor for non-obese non-alcoholic fatty liver disease. *Aliment Pharmacol Ther*. 2017;45(11):1403-1412. doi:10.1111/apt.14058
20. Wu J, Yao XY, Shi RX, Liu SF, Wang XY. A potential link between polycystic ovary syndrome and non-alcoholic fatty liver disease: an update meta-analysis. *Reprod Health*. 2018;15(1):77. doi:10.1186/s12978-018-0519-2
21. Gambarin-Gelwan M, Kinkhabwala SV, Schiano TD, Bodian C, Yeh HC, Futterweit W. Prevalence of nonalcoholic fatty liver disease in women with polycystic ovary syndrome. *Clin Gastroenterol Hepatol*. 2007;5(4):496-501. doi:10.1016/j.cgh.2006.10.010
22. Karoli R, Fatima J, Chandra A, Gupta U, Islam FU, Singh G. Prevalence of hepatic steatosis in women with polycystic ovary syndrome. *J Hum Reprod Sci*. 2013;6(1):9-14. doi:10.4103/0974-1208.112370
23. Kumarendran B, O'Reilly MW, Manolopoulos KN, *et al*. Polycystic ovary syndrome, androgen excess, and the risk of nonalcoholic fatty liver disease in women: a longitudinal study based on a United Kingdom primary care database. *PLoS Med*. 2018;15(3):e1002542. doi:10.1371/journal.pmed.1002542
24. Vassilatou E, Lafoyianni S, Vryonidou A, *et al*. Increased androgen bioavailability is associated with non-alcoholic fatty liver disease in women with polycystic ovary syndrome. *Hum Reprod*. 2010;25(1):212-220. doi:10.1093/humrep/dep380
25. Rocha ALL, Faria LC, Guimaraes TCM, *et al*. Non-alcoholic fatty liver disease in women with polycystic ovary syndrome: systematic review and meta-analysis. *J Endocrinol Invest*. 2017;40(12):1279-1288. doi:10.1007/s40618-017-0708-9
26. Jones H, Sprung VS, Pugh CJ, *et al*. Polycystic ovary syndrome with hyperandrogenism is characterized by an increased risk of hepatic steatosis compared to nonhyperandrogenic PCOS phenotypes and healthy controls, independent of obesity and insulin resistance. *J*

Clin Endocrinol Metab. 2012;97(10):3709-3716. doi:10.1210/jc.2012-1382
27. Won YB, Seo SK, Yun BH, Cho S, Choi YS, Lee BS. Non-alcoholic fatty liver disease in polycystic ovary syndrome women. *Sci Rep*. 2021;11(1):7085. doi:10.1038/s41598-021-86697-y
28. Cai J, Wu CH, Zhang Y, *et al*. High-free androgen index is associated with increased risk of non-alcoholic fatty liver disease in women with polycystic ovary syndrome, independent of obesity and insulin resistance. *Int J Obes (Lond)*. 2017;41(9):1341-1347. doi:10.1038/ijo.2017.116
29. Sarwar R, Pierce N, Koppe S. Obesity and nonalcoholic fatty liver disease: current perspectives. *Diabetes Metab Syndr Obes*. 2018;11:533-542. doi:10.2147/DMSO.S146339
30. Hammes SR, Levin ER. Extranuclear steroid receptors: nature and actions. *Endocr Rev*. 2007;28(7):726-741. doi:10.1210/er.2007-0022
31. Foradori CD, Weiser MJ, Handa RJ. Non-genomic actions of androgens. *Front Neuroendocrinol*. 2008;29(2):169-181. doi:10.1016/j.yfrne.2007.10.005
32. Michels G, Hoppe UC. Rapid actions of androgens. *Front Neuroendocrinol*. 2008;29(2):182-198. doi:10.1016/j.yfrne.2007.08.004
33. Ma X, Hayes E, Biswas A, *et al*. Androgens regulate ovarian gene expression through modulation of ezh2 expression and activity. *Endocrinology*. 2017;158(9):2944-2954. doi:10.1210/en.2017-00145
34. Roy S, Huang B, Sinha N, Wang J, Sen A. Androgens regulate ovarian gene expression by balancing Ezh2-Jmjd3 mediated H3K27me3 dynamics. *PLoS Genet*. 2021;17(3):e1009483. doi:10.1371/journal.pgen.1009483
35. Sen A, Prizant H, Light A, *et al*. Androgens regulate ovarian follicular development by increasing follicle stimulating hormone receptor and microRNA-125b expression. *Proc Natl Acad Sci USA*. 2014;111(8):3008-3013. doi:10.1073/pnas.1318978111
36. van Houten EL, Kramer P, McLuskey A, Karels B, Themmen AP, Visser JA. Reproductive and metabolic phenotype of a mouse model of PCOS. *Endocrinology*. 2012;153(6):2861-2869. doi:10.1210/en.2011-1754
37. Caldwell AS, Middleton LJ, Jimenez M, *et al*. Characterization of reproductive, metabolic, and endocrine features of polycystic ovary syndrome in female hyperandrogenic mouse models. *Endocrinology*. 2014;155(8):3146-3159. doi:10.1210/en.2014-1196
38. Sen A, Hammes SR. Granulosa cell-specific androgen receptors are critical regulators of ovarian development and function. *Mol Endocrinol*. 2010;24(7):1393-1403. doi:10.1210/me.2010-0006
39. Postic C, Shiota M, Niswender KD, *et al*. Dual roles for glucokinase in glucose homeostasis as determined by liver and pancreatic beta cell-specific gene knock-outs using Cre recombinase. *J Biol Chem*. 1999;274(1):305-315. doi:10.1074/jbc.274.1.305
40. Tsuru H, Osaka M, Hiraoka Y, Yoshida M. HFD-induced hepatic lipid accumulation and inflammation are decreased in factor D deficient mouse. *Sci Rep*. 2020;10(1):17593. doi:10.1038/s41598-020-74617-5
41. Lydic TA, Busik JV, Reid GE. A monophasic extraction strategy for the simultaneous lipidome analysis of polar and nonpolar retina lipids. *J Lipid Res*. 2014;55(8):1797-1809. doi:10.1194/jlr.D050302
42. Evaul K, Hammes SR. Cross-talk between G protein-coupled and epidermal growth factor receptors regulates gonadotropin-mediated steroidogenesis in Leydig cells. *J Biol Chem*. 2008;283(41):27525-27533. doi:10.1074/jbc.M803867200
43. Roy S, Gandra D, Seger C, *et al*. Oocyte-derived factors (GDF9 and BMP15) and FSH regulate AMH expression via modulation of H3K27AC in granulosa cells. *Endocrinology*. 2018;159(9):3433-3445. doi:10.1210/en.2018-00609
44. Sinha N, Roy S, Huang B, Wang J, Padmanabhan V, Sen A. Developmental programming: prenatal testosterone-induced epigenetic modulation and its effect on gene expression in sheep ovarydagger. *Biol Reprod*. 2020;102(5):1045-1054. doi:10.1093/biolre/ioaa007
45. RRID:AB_10694383. https://scicrunch.org/resolver/RRID:AB_10694383
46. RRID:AB_2909496. https://scicrunch.org/resolver/RRID:AB_2909496
47. RRID:AB_2909497. https://scicrunch.org/resolver/RRID:AB_2909497
48. RRID:AB_2616029. https://scicrunch.org/resolver/RRID:AB_2616029
49. RRID:AB_331563. https://scicrunch.org/resolver/RRID:AB_331563
50. RRID:AB_1280747. https://scicrunch.org/resolver/RRID:AB_1280747
51. RRID:AB_303729. https://scicrunch.org/resolver/RRID:AB_303729
52. Roy S, Aierken A, Salinas I, *et al*. Supplementary data for: Androgen-mediated perturbation of hepatic circadian system through epigenetic modulation promotes NAFLD in PCOS mice. *figshare*. Deposited June 4, 2022. doi:10.6084/m9.figshare.19522387.v1
53. Sen A, De Castro I, Defranco DB, *et al*. Paxillin mediates extranuclear and intranuclear signaling in prostate cancer proliferation. *J Clin Invest*. 2012;122(7):2469-2481. doi:10.1172/JCI62044
54. RRID:AB_305237. https://scicrunch.org/resolver/RRID:AB_305237
55. Yoo SH, Yamazaki S, Lowrey PL, *et al*. PERIOD2::LUCIFERASE real-time reporting of circadian dynamics reveals persistent circadian oscillations in mouse peripheral tissues. *Proc Natl Acad Sci USA*. 2004;101(15):5339-5346. doi:10.1073/pnas.0308709101
56. True CA, Takahashi DL, Burns SE, *et al*. Chronic combined hyperandrogenemia and Western-style diet in young female rhesus macaques causes greater metabolic impairments compared to either treatment alone. *Hum Reprod*. 2017;32(9):1880-1891. doi:10.1093/humrep/dex246
57. Bishop CV, Takahashi D, Mishler E, *et al*. Individual and combined effects of 5-year exposure to hyperandrogenemia and Western-style diet on metabolism and reproduction in female rhesus macaques. *Hum Reprod*. 2021;36(2):444-454. doi:10.1093/humrep/deaa321
58. Walters KA. Androgens in polycystic ovary syndrome: lessons from experimental models. *Curr Opin Endocrinol Diabetes Obes*. 2016;23(3):257-263. doi:10.1097/MED.0000000000000245
59. Walters KA, Allan CM, Handelsman DJ. Rodent models for human polycystic ovary syndrome. *Biol Reprod*. 2012;86(5):149, 1-12. doi:10.1095/biolreprod.111.097808
60. Walters KA, Bertoldo MJ, Handelsman DJ. Evidence from animal models on the pathogenesis of PCOS. *Best Pract Res Clin Endocrinol Metab*. 2018;32(3):271-281. doi:10.1016/j.beem.2018.03.008
61. Stener-Victorin E, Padmanabhan V, Walters KA, *et al*. Animal models to understand the etiology and pathophysiology of polycystic ovary syndrome. *Endocr Rev*. 2020;**41**(4):bnaa010. doi:10.1210/endrev/bnaa010
62. Lin HY, Yu IC, Wang RS, *et al*. Increased hepatic steatosis and insulin resistance in mice lacking hepatic androgen receptor. *Hepatology*. 2008;47(6):1924-1935. doi:10.1002/hep.22252
63. Sans A, Bonnafous S, Rousseau D, *et al*. The differential expression of Cide family members is associated with Nafld progression from steatosis to steatohepatitis. *Sci Rep*. 2019;9(1):7501. doi:10.1038/s41598-019-43928-7
64. Skat-Rordam J, Hojland Ipsen D, Lykkesfeldt J, Tveden-Nyborg P. A role of peroxisome proliferator-activated receptor gamma in non-alcoholic fatty liver disease. *Basic Clin Pharmacol Toxicol*. 2019;124(5):528-537. doi:10.1111/bcpt.13190
65. Rusli F, Deelen J, Andriyani E, *et al*. Fibroblast growth factor 21 reflects liver fat accumulation and dysregulation of signalling pathways in the liver of C57BL/6J mice. *Sci Rep*. 2016;6:30484. doi:10.1038/srep30484
66. Tillman EJ, Rolph T. FGF21: an emerging therapeutic target for non-alcoholic steatohepatitis and related metabolic diseases. *Front Endocrinol (Lausanne)*. 2020;11:601290. doi:10.3389/fendo.2020.601290
67. Orlicky DJ, Libby AE, Bales ES, *et al*. Perilipin-2 promotes obesity and progressive fatty liver disease in mice through mechanistically distinct hepatocyte and extra-hepatocyte actions. *J Physiol*. 2019;597(6):1565-1584. doi:10.1113/JP277140
68. Soufi N, Hall AM, Chen Z, *et al*. Inhibiting monoacylglycerol acyltransferase 1 ameliorates hepatic metabolic abnormalities but not inflammation and injury in mice. *J Biol Chem*. 2014;289(43):30177-30188. doi:10.1074/jbc.M114.595850
69. Liss KHH, Ek SE, Lutkewitte AJ, *et al*. Monoacylglycerol acyltransferase 1 knockdown exacerbates hepatic ischemia/

reperfusion injury in mice with hepatic steatosis. *Liver Transpl.* 2021;27(1):116-133. doi:10.1002/lt.25886
70. Nwosu ZC, Megger DA, Hammad S, *et al*. Identification of the consistently altered metabolic targets in human hepatocellular carcinoma. *Cell Mol Gastroenterol Hepatol.* 2017;4(2):303-323.e1. doi:10.1016/j.jcmgh.2017.05.004
71. Hall Z, Bond NJ, Ashmore T, *et al*. Lipid zonation and phospholipid remodeling in nonalcoholic fatty liver disease. *Hepatology.* 2017;65(4):1165-1180. doi:10.1002/hep.28953
72. Martin J, Maurhofer O, Bellance N, *et al*. Disruption of the histidine triad nucleotide-binding hint2 gene in mice affects glycemic control and mitochondrial function. *Hepatology.* 2013;57(5):2037-2048. doi:10.1002/hep.26060
73. Nabeshima A, Yamada S, Guo X, *et al*. Peroxiredoxin 4 protects against nonalcoholic steatohepatitis and type 2 diabetes in a nongenetic mouse model. *Antioxid Redox Signal.* 2013;19(17):1983-1998. doi:10.1089/ars.2012.4946
74. Richards J, Gumz ML. Mechanism of the circadian clock in physiology. *Am J Physiol Regul Integr Comp Physiol.* 2013;304(12):R1053-R1064. doi:10.1152/ajpregu.00066.2013
75. Qian J, Scheer FA. Circadian system and glucose metabolism: implications for physiology and disease. *Trends Endocrinol Metab.* 2016;27(5):282-293. doi:10.1016/j.tem.2016.03.005
76. Eckel-Mahan K, Sassone-Corsi P. Metabolism and the circadian clock converge. *Physiol Rev.* 2013;93(1):107-135. doi:10.1152/physrev.00016.2012
77. Reinke H, Asher G. Circadian clock control of liver metabolic functions. *Gastroenterology.* 2016;150(3):574-580. doi:10.1053/j.gastro.2015.11.043
78. Sookoian S, Castano G, Gemma C, Gianotti TF, Pirola CJ. Common genetic variations in CLOCK transcription factor are associated with nonalcoholic fatty liver disease. *World J Gastroenterol.* 2007;13(31):4242-4248. doi:10.3748/wjg.v13.i31.4242
79. Mohawk JA, Green CB, Takahashi JS. Central and peripheral circadian clocks in mammals. *Annu Rev Neurosci.* 2012;35:445-462. doi:10.1146/annurev-neuro-060909-153128
80. Tahara Y, Shibata S. Circadian rhythms of liver physiology and disease: experimental and clinical evidence. *Nat Rev Gastroenterol Hepatol.* 2016;13(4):217-226. doi:10.1038/nrgastro.2016.8
81. Wolk R, Gami AS, Garcia-Touchard A, Somers VK. Sleep and cardiovascular disease. *Curr Probl Cardiol.* 2005;30(12):625-662. doi:10.1016/j.cpcardiol.2005.07.002
82. Husse J, Hintze SC, Eichele G, Lehnert H, Oster H. Circadian clock genes Per1 and Per2 regulate the response of metabolism-associated transcripts to sleep disruption. *PLoS One.* 2012;7(12):e52983. doi:10.1371/journal.pone.0052983
83. Pinola P, Piltonen TT, Puurunen J, *et al*. Androgen profile through life in women with polycystic ovary syndrome: a Nordic multicenter collaboration study. *J Clin Endocrinol Metab.* 2015;100(9):3400-3407. doi:10.1210/jc.2015-2123
84. Pasquali R, Zanotti L, Fanelli F, *et al*. Defining hyperandrogenism in women with polycystic ovary syndrome: a challenging perspective. *J Clin Endocrinol Metab.* 2016;101(5):2013-2022. doi:10.1210/jc.2015-4009
85. Welt CK, Gudmundsson JA, Arason G, *et al*. Characterizing discrete subsets of polycystic ovary syndrome as defined by the Rotterdam criteria: the impact of weight on phenotype and metabolic features. *J Clin Endocrinol Metab.* 2006;91(12):4842-4848. doi:10.1210/jc.2006-1327
86. Welt CK, Arason G, Gudmundsson JA, *et al*. Defining constant versus variable phenotypic features of women with polycystic ovary syndrome using different ethnic groups and populations. *J Clin Endocrinol Metab.* 2006;91(11):4361-4368. doi:10.1210/jc.2006-1191
87. Andrisse S, Feng M, Wang Z, *et al*. Androgen-induced insulin resistance is ameliorated by deletion of hepatic androgen receptor in females. *FASEB J.* 2021;35(10):e21921. doi:10.1096/fj.202100961R
88. Andrisse S, Childress S, Ma Y, *et al*. Low-dose dihydrotestosterone drives metabolic dysfunction via cytosolic and nuclear hepatic androgen receptor mechanisms. *Endocrinology.* 2017;158(3):531-544. doi:10.1210/en.2016-1553
89. Cox MJ, Edwards MC, Rodriguez Paris V, *et al*. Androgen action in adipose tissue and the brain are key mediators in the development of PCOS traits in a mouse model. *Endocrinology.* 2020;161(7):bqaa061. doi:10.1210/endocr/bqaa061
90. Inoue M, Ohtake T, Motomura W, *et al*. Increased expression of PPARgamma in high fat diet-induced liver steatosis in mice. *Biochem Biophys Res Commun.* 2005;336(1):215-222. doi:10.1016/j.bbrc.2005.08.070
91. Zhou J, Febbraio M, Wada T, *et al*. Hepatic fatty acid transporter Cd36 is a common target of LXR, PXR, and PPARgamma in promoting steatosis. *Gastroenterology.* 2008;134(2):556-567.e1. doi:10.1053/j.gastro.2007.11.037
92. Gritsina G, Gao WQ, Yu J. Transcriptional repression by androgen receptor: roles in castration-resistant prostate cancer. *Asian J Androl.* 2019;21(3):215-223. doi:10.4103/aja.aja_19_19
93. Tezze C, Romanello V, Sandri M. FGF21 as modulator of metabolism in health and disease. *Front Physiol.* 2019;10:419. doi:10.3389/fphys.2019.00419
94. Tucker B, Li H, Long X, Rye KA, Ong KL. Fibroblast growth factor 21 in non-alcoholic fatty liver disease. *Metabolism.* 2019;101:153994. doi:10.1016/j.metabol.2019.153994
95. Vgontzas AN, Legro RS, Bixler EO, Grayev A, Kales A, Chrousos GP. Polycystic ovary syndrome is associated with obstructive sleep apnea and daytime sleepiness: role of insulin resistance. *J Clin Endocrinol Metab.* 2001;86(2):517-520. doi:10.1210/jcem.86.2.7185
96. Shreeve N, Cagampang F, Sadek K, *et al*. Poor sleep in PCOS; is melatonin the culprit? *Hum Reprod.* 2013;28(5):1348-1353. doi:10.1093/humrep/det013
97. Jain P, Jain M, Haldar C, Singh TB, Jain S. Melatonin and its correlation with testosterone in polycystic ovarian syndrome. *J Hum Reprod Sci.* 2013;6(4):253-258. doi:10.4103/0974-1208.126295
98. Crowley SJ, Van Reen E, LeBourgeois MK, *et al*. A longitudinal assessment of sleep timing, circadian phase, and phase angle of entrainment across human adolescence. *PLoS One.* 2014;9(11):e112199e112199. doi:10.1371/journal.pone.0112199
99. Wang F, Xie N, Wu Y, *et al*. Association between circadian rhythm disruption and polycystic ovary syndrome. *Fertil Steril.* 2020
100. Moore RY. Circadian rhythms: basic neurobiology and clinical applications. *Annu Rev Med.* 1997;48:253-266. doi:10.1146/annurev.med.48.1.253
101. Partch CL, Green CB, Takahashi JS. Molecular architecture of the mammalian circadian clock. *Trends Cell Biol.* 2014;24(2):90-99. doi:10.1016/j.tcb.2013.07.002
102. Patel SR, Hu FB. Short sleep duration and weight gain: a systematic review. *Obesity.* 2008;16(3):643-653. doi:10.1038/oby.2007.118
103. Cappuccio FP, Taggart FM, Kandala NB, *et al*. Meta-analysis of short sleep duration and obesity in children and adults. *Sleep.* 2008;31(5):619-626. doi:10.1093/sleep/31.5.619
104. Broussard JL, Ehrmann DA, Van Cauter E, Tasali E, Brady MJ. Impaired insulin signaling in human adipocytes after experimental sleep restriction: a randomized, crossover study. *Ann Intern Med.* 2012;157(8):549-557. doi:10.7326/0003-4819-157-8-201210160-00005
105. Sciarra F, Franceschini E, Campolo F, *et al*. Disruption of circadian rhythms: a crucial factor in the etiology of infertility. *Int J Mol Sci* . 2020;21(11):3943. doi:10.3390/ijms21113943
106. Simon SL, McWhirter L, Diniz Behn C, *et al*. Morning circadian misalignment is associated with insulin resistance in girls with obesity and polycystic ovarian syndrome. *J Clin Endocrinol Metab.* 2019;104(8):3525-3534. doi:10.1210/jc.2018-02385
107. Li S, Zhai J, Chu W, Geng X, Chen ZJ, Du Y. Altered circadian clock as a novel therapeutic target for constant darkness-induced insulin resistance and hyperandrogenism of polycystic ovary syndrome. *Transl Res.* 2020;219:13-29. doi:10.1016/j.trsl.2020.02.003

108. Han S, Zhang R, Jain R, *et al*. Circadian control of bile acid synthesis by a KLF15-Fgf15 axis. *Nat Commun*. 2015;6:7231. doi:10.1038/ncomms8231
109. Arab JP, Karpen SJ, Dawson PA, Arrese M, Trauner M. Bile acids and nonalcoholic fatty liver disease: molecular insights and therapeutic perspectives. *Hepatology*. 2017;65(1):350-362. doi:10.1002/hep.28709
110. Miller BH, McDearmon EL, Panda S, *et al*. Circadian and CLOCK-controlled regulation of the mouse transcriptome and cell proliferation. *Proc Natl Acad Sci USA*. 2007;104(9):3342-3347. doi:10.1073/pnas.0611724104
111. Takahashi JS. Transcriptional architecture of the mammalian circadian clock. *Nat Rev Genet*. 2017;18(3):164-179. doi:10.1038/nrg.2016.150
112. Gilardi F, Migliavacca E, Naldi A, *et al*. Genome-wide analysis of SREBP1 activity around the clock reveals its combined dependency on nutrient and circadian signals. *PLoS Genet*. 2014;10(3):e1004155. doi:10.1371/journal.pgen.1004155
113. Mazzoccoli G, Vinciguerra M, Oben J, Tarquini R, De Cosmo S. Non-alcoholic fatty liver disease: the role of nuclear receptors and circadian rhythmicity. *Liver Int*. 2014;34(8):1133-1152. doi:10.1111/liv.12534
114. Mereness AL, Murphy ZC, Sellix MT. Developmental programming by androgen affects the circadian timing system in female mice. *Biol Reprod*. 2015;92(4):88. doi:10.1095/biolreprod.114.126409
115. Salinas I, Sinha N, Sen A. Androgen-induced epigenetic modulations in the ovary. *J Endocrinol*. 2021;**249**(3):R53-R64. doi:10.1530/JOE-20-0578
116. Sherry-Lynes MM, Sengupta S, Kulkarni S, Cochran BH. Regulation of the JMJD3 (KDM6B) histone demethylase in glioblastoma stem cells by STAT3. *PLoS One*. 2017;12(4):e0174775. doi:10.1371/journal.pone.0174775
117. Pan D, Huang L, Zhu LJ, *et al*. Jmjd3-mediated H3K27me3 dynamics orchestrate brown fat development and regulate white fat plasticity. *Dev Cell*. 2015;35(5):568-583. doi:10.1016/j.devcel.2015.11.002
118. Vella S, Gnani D, Crudele A, *et al*. EZH2 down-regulation exacerbates lipid accumulation and inflammation in in vitro and in vivo NAFLD. *Int J Mol Sci* . 2013;14(12):24154-24168. doi:10.3390/ijms141224154